PLOS GENETICS

RESEARCH ARTICLE

Mutation of NEKL-4/NEK10 and TTLL genes suppress neuronal ciliary degeneration caused by loss of CCPP-1 deglutamylase function

Kade M. Power[1], Jyothi S. Akella[1], Amanda Gu[1], Jonathon D. Walsh[1], Sebastian Bellotti[1], Margaret Morash[1], Winnie Zhang[1], Yasmin H. Ramadan[1], Nicole Ross[2], Andy Golden[3], Harold E. Smith[3], Maureen M. Barr[1]*, Robert O'Hagan[2]*

1 Department of Genetics and Human Genetics Institute of New Jersey, Rutgers University, Piscataway, NJ, United States of America, **2** Biology Department, Montclair State University, Montclair, NJ, United States of America, **3** National Institute of Diabetes and Digestive and Kidney Diseases, National Institutes of Health, Bethesda, Maryland, United States of America

* barr@dls.rutgers.edu (MMB); ohaganr@montclair.edu (RO)

Citation: Power KM, Akella JS, Gu A, Walsh JD, Bellotti S, Morash M, et al. (2020) Mutation of NEKL-4/NEK10 and TTLL genes suppress neuronal ciliary degeneration caused by loss of CCPP-1 deglutamylase function. PLoS Genet 16(10): e1009052. https://doi.org/10.1371/journal.pgen.1009052

Editor: Susan K. Dutcher, Washington University School of Medicine, UNITED STATES

Received: May 22, 2020

Accepted: August 14, 2020

Published: October 16, 2020

Data Availability Statement: All relevant data are within the manuscript and its Supporting Information files.

Funding: This work was funded by the New Jersey Commission for Spinal Cord Research (NJCSCR) CSCR15IRG014 to R. O.; NIH DK116606 to M. M. B.; NIH Institutional Research and Academic Career Development Award (IRACDA) K12GM093854 to J. D. W; and the Intramural Research Program of the National Institutes of Health, National Institute

Abstract

Ciliary microtubules are subject to post-translational modifications that act as a "Tubulin Code" to regulate motor traffic, binding proteins and stability. In humans, loss of CCP1, a cytosolic carboxypeptidase and tubulin deglutamylating enzyme, causes infantile-onset neurodegeneration. In *C. elegans*, mutations in *ccpp-1*, the homolog of CCP1, result in progressive degeneration of neuronal cilia and loss of neuronal function. To identify genes that regulate microtubule glutamylation and ciliary integrity, we performed a forward genetic screen for suppressors of ciliary degeneration in *ccpp-1* mutants. We isolated the *ttll-5 (my38)* suppressor, a mutation in a tubulin tyrosine ligase-like glutamylase gene. We show that mutation in the *ttll-4*, *ttll-5*, or *ttll-11* gene suppressed the hyperglutamylation-induced loss of ciliary dye filling and kinesin-2 mislocalization in *ccpp-1* cilia. We also identified the *nekl-4(my31)* suppressor, an allele affecting the NIMA (Never in Mitosis A)-related kinase NEKL-4/NEK10. In humans, NEK10 mutation causes bronchiectasis, an airway and muco-ciliary transport disorder caused by defective motile cilia. *C. elegans* NEKL-4 localizes to the ciliary base but does not localize to cilia, suggesting an indirect role in ciliary processes. This work defines a pathway in which glutamylation, a component of the Tubulin Code, is written by TTLL-4, TTLL-5, and TTLL-11; is erased by CCPP-1; is read by ciliary kinesins; and its downstream effects are modulated by NEKL-4 activity. Identification of regulators of microtubule glutamylation in diverse cellular contexts is important to the development of effective therapies for disorders characterized by changes in microtubule glutamylation. By identifying *C. elegans* genes important for neuronal and ciliary stability, our work may inform research into the roles of the tubulin code in human ciliopathies and neurodegenerative diseases.

of Diabetes and Digestive and Kidney Diseases (NIDDK) (H.S. and A.G.). The funders had no role in study design, data collection and analysis, decision to publish, or preparation of the manuscript.

Competing interests: The authors have declared that no competing interests exist.

Author summary

Cilia are microtubule-based organelles that play essential roles in human development and health. Ciliopathies are caused by abnormalities in the structure or function of primary cilia, with polycystic kidney disease (PKD) being a common clinical phenotype. As cilia are found on most non-dividing cells in the human body, ciliopathies often display extrarenal manifestations including neurological disorders and retinal degeneration. The Tubulin Code–combinatorial use of tubulin isotypes and post-translational modifications–dictates ciliary structure, motor-based transport, and function. Mutation in the tubulin deglutamylase *ccpp-1* (cytosolic carboxypeptidase) results in ciliary hyperglutamylation and degeneration. *C. elegans ccpp-1* ciliary degeneration is suppressed by a mutation in any of three TTLL (tubulin tyrosine ligase-like) glutamylase genes, indicating that regulated glutamylation is critically important for ciliary homeostasis. Pathological hyperglutamylation caused by CCP deglutamylase mutations are associated with human retinal degeneration and murine progressive neurodegeneration and sperm immotility. *ccpp-1* ciliary degeneration is also suppressed by a mutation in the kinase NEKL-4/NEK10. NEK kinases are implicated in polycystic kidney disease and other ciliopathies and NEKL-4/NEK10 is important for ciliary stability in *C. elegans*. By identifying *C. elegans* genes important for neuronal and ciliary stability, "the worm" may inform research into human ciliopathies and neurodegenerative diseases.

Introduction

Cilia and flagella are antenna-like organelles that are conserved from algae to humans and play important roles in sensation, intercellular communication, development, and homeostasis [1]. The core of both cilia and flagella is the axoneme, a conserved microtubule structure with a ring of nine doublets that may surround inner microtubule singlets in motile cilia [1]. The Tubulin Code hypothesis suggests that post-translational modifications, such as glutamylation, acetylation, glycylation, detyrosination, and others, can increase the diversity of microtubules beyond incorporation of different tubulin isotypes for structural and functional specialization [2].

Glutamylation, or addition of side-chains of the amino acid glutamate, of tubulin tails is emerging as an important factor in organizing the microtubule cytoskeleton [3,4]. Microtubules in neurons and cilia can be reversibly glutamylated. Although the function of glutamylation and other post-translational modifications is not completely understood, enzymes that regulate post-translational glutamylation of microtubules are known. Cytosolic carboxypeptidases (CCPs) such as CCP1 deglutamylate microtubules [5,6], opposing the activity of tubulin tyrosine ligase-like (TTLL) enzymes, which add glutamates to tubulin tails [7–9]. Glutamylation side-chains can be as short as a single glutamate, or as long as 20 glutamates [10]. Particular CCP enzymes may reduce the length of glutamate side-chains, and some can remove the branch point glutamate to eliminate glutamylation [5]. Similarly, some TTLL family members initiate glutamate side-chains, while others elongate [9]. TTLLs may also have preferences for α or β tubulin substrates [9]. Therefore, microtubule glutamylation is not uniform, and both side-chain length and tubulin substrate may exert different influences over motors, microtubule-associated proteins (MAPs), or other regulators of microtubule stability.

Glutamylation is essential for neuronal survival and axoneme stability, and a growing list of reports link hyper- or hypo-glutamylation to disease. Dysregulated microtubule glutamylation

causes infantile-onset neurodegeneration and the ciliopathy Joubert syndrome in humans, and progressive cerebellar purkinje cell degeneration (*pcd*) in mice [3,5,11–14]. Defects in axonal transport, which may be regulated by the Tubulin Code, contribute to neurodegenerative diseases including Alzheimer's disease and Parkinson's disease [4,15]. Although the importance of regulated glutamylation on ciliary and neuronal microtubules are clearly established, a comprehensive understanding of microtubule glutamylation is necessary to understand and interpret its context-specific effects in different cilia and neuron types.

The nematode *C. elegans* offers advantages to unraveling the Tubulin Code. Most basic biological processes, including axon development, neuronal transport, and ciliogenesis are conserved between *C. elegans* and humans [16]. In the worm, cilia are located on the distal most ends of sensory dendrites [17–19], are not essential for viability, and are diverse in terms of the composition and arrangement of microtubules, tubulin post-translational modifications, and motor proteins [2,18,20]. In male-specific ciliated sensory neurons, the CCPP-1 deglutamylase and TTLL-11 glutamylase control ciliary ultrastructure and particular ciliary kinesin motors [21,22]. In amphid and phasmid sensory neurons, loss of CCPP-1 leads to degeneration of ciliary microtubules indicating cell-specific differences in the tubulin code [21,22].

In *C. elegans* amphid and phasmid neurons, ciliary integrity is easily tested using a dye-filling assay [18]. *ccpp-1* mutants are dye-filling defective (Dyf) in adults but not early larval stages, reflecting ultrastructural defects and progressive ciliary microtubule degeneration [21]. Using a candidate gene approach, we found that deletion mutations in *ttll-4*, *ttll-5*, or *ttll-11* glutamylase genes suppressed the *ccpp-1* Dyf phenotype. To identify new molecules and pathways that function in ciliary homeostasis, we performed a genetic screen for mutations that suppress the *ccpp-1* Dyf phenotype. We identified mutations in *ttll-5* and in the never-in-mitosis kinase gene *nekl-4*. In humans, TTLL5 mutation causes recessive retinal dystrophy [23,24]. *C. elegans* NEKL-4 is homologous to human NEK10, which is a kinase specific to ciliated cells and contributes to ciliogenesis in cultured human kidney cells [25]. In humans, NEK10 mutation causes bronchiectasis, a disorder of mucociliary transport in the airway due to defective motile cilia [26]. Here we show that NEKL-4 is expressed in all ciliated neurons but does not localize to cilia, suggesting that NEKL-4 indirectly influences regulation of ciliary stability. This work represents a step toward elucidating the molecular pathways by which glutamylation, as a component of the Tubulin Code, regulates cilia; this, in turn, allows us to better understand ciliopathies and neuronal survival in humans.

Results

Single gene mutations in glutamylases *ttll-4*, *ttll-5*, and *ttll-11* suppress the *ccpp-1* dye-filling defect

ccpp-1 mutation causes hyperglutamylation and progressive ciliary degeneration in amphid and phasmid neuronal cilia ([21]; **Fig 1A**). Ciliary degeneration is detectable using dye-filling assays, in which *C. elegans* nematodes are soaked in the fluorescent lipophilic dye DiI (**Fig 1B**). The dye is only taken up in neurons that have intact sensory cilia; therefore, adult *ccpp-1* do not take up this fluorescent dye and display the Dye-filling defective, or "Dyf," phenotype ([21]; **Fig 1C**).

We first tested candidate genes for suppression of the *ccpp-1* Dyf phenotype. Glutamylases of the tubulin tyrosine ligase-like TTLL family oppose CCP deglutamylase function [27]. The *C. elegans* genome encodes five TTLL glutamylases—*ttll-4*, *ttll-5*, *ttll-9*, *ttll-11*, and *ttll-15* [6,28]. We previously showed that *ttll-4* mutation suppresses the *ccpp-1* Dyf defect, suggesting that TTLL-4 glutamylates microtubules in amphid and phasmid cilia [21]. We therefore tested deletion alleles in the other *ttll* genes and found that deletion mutations in *ttll-5* and *ttll-11*

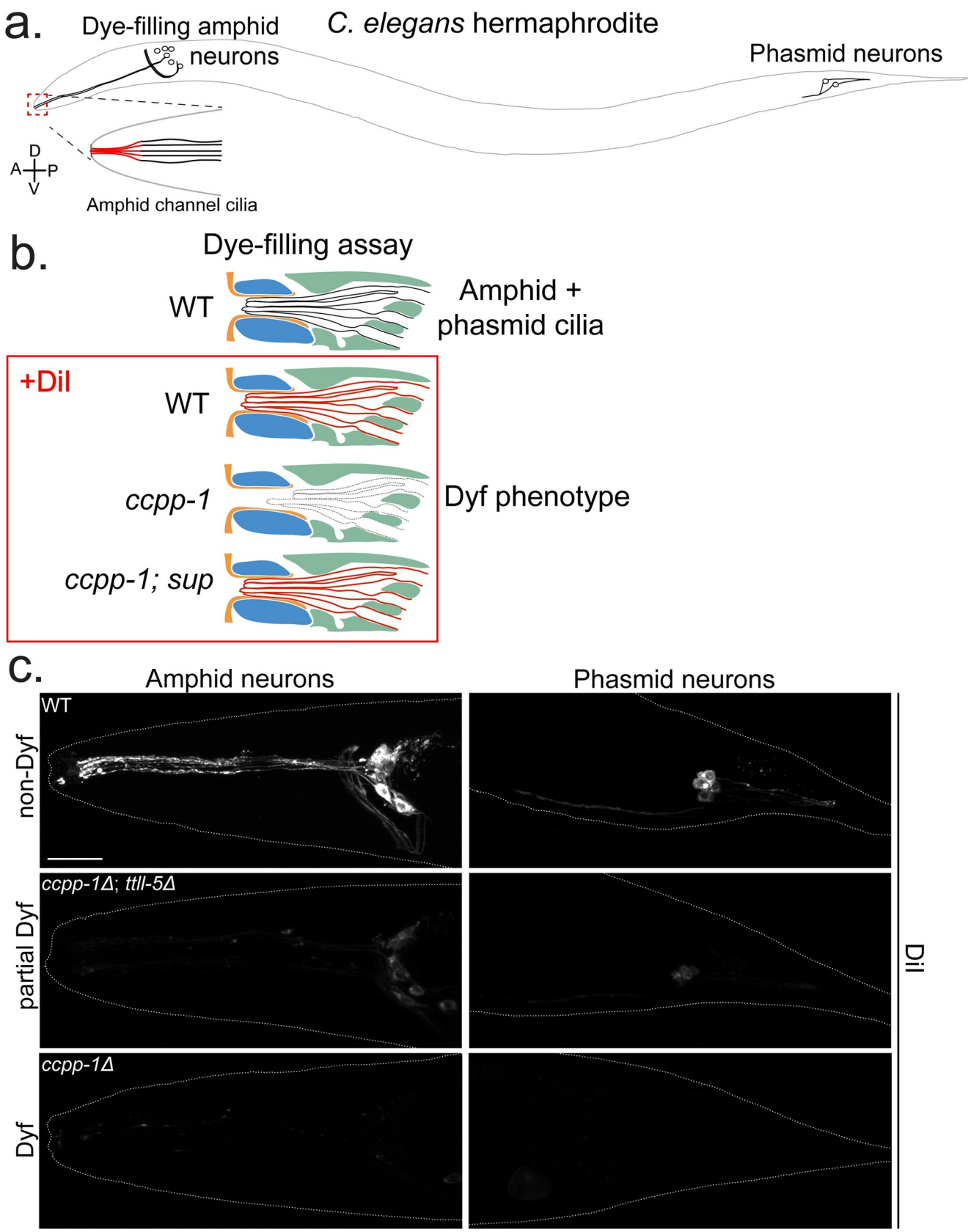
a.
Dye-filling amphid neurons
C. elegans hermaphrodite
Phasmid neurons
D
A
P
V
Amphid channel cilia
b.
Dye-filling assay
WT
Amphid + phasmid cilia
+DiI
WT
ccpp-1
ccpp-1; sup
Dyf phenotype
c.
Amphid neurons
Phasmid neurons
WT
non-Dyf
ccpp-1Δ; ttll-5Δ
partial Dyf
ccpp-1Δ
Dyf
DiI

Fig 1. Overview of Dye-filling assays and examples of observed phenotypes. a. Diagram of a *C. elegans* hermaphrodite highlighting the amphid and phasmid sensory neurons, which absorb dye through their cilia. Inset shows the amphid channel cilia (adapted from *O'Hagan et al* [22]). **b.** Illustration of the dye-filling assays. DiI is a lipophilic fluorescent dye that is taken up by the cilia. **c.** Examples of non-Dyf, partial Dyf, and Dyf phenotypes. Scale = 10μm.

https://doi.org/10.1371/journal.pgen.1009052.g001

suppressed the Dyf defect of *ccpp-1* (Fig 2A). The *ttll-4* gene encodes two protein isoforms by alternative splicing, TTLL-4A (601 AA) and TTLL-4B (563 AA) (Fig 2B; [29]). Both isoforms contain a TTL domain (amino acid residues 138–476 in TTLL-4A; 100–438 in TTLL-4B) that is conserved among other TTLL genes. To study *ttll-4*, we used the *tm3310* allele, containing a

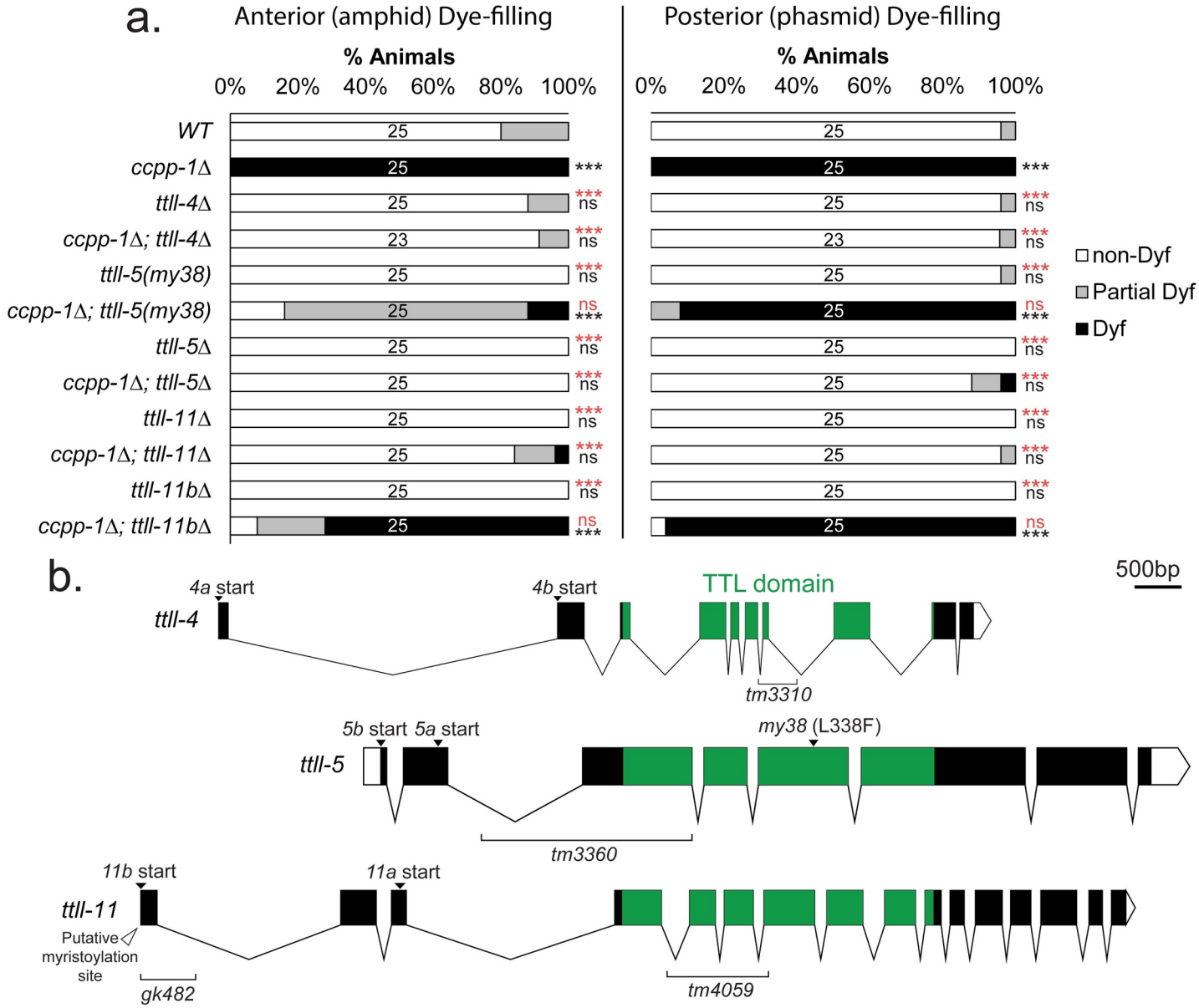

Fig 2. *ttll-4*, *ttll-5* and *ttll-11* act as suppressors of the *ccpp-1* Dyf phenotype. a. Suppression of *ccpp-1* Dyf phenotype by *ttll-4*, *ttll-5* and *ttll-11*. All strains marked with *Δ* are deletion alleles. *ttll-11bΔ* refers to the *ttll-11b(gk482)* allele. N of animals per strain is indicated on bars. *** indicates $p \leq 0.0001$ by Kruskal-Wallis one-way ANOVA analysis and post hoc Dunn's multiple comparison test. Black indicates significance relative to wild type and red indicates significance relative to *ccpp-1Δ*. **b.** Gene diagrams of *ttll-4*, *ttll-5* and *ttll-11*, aligned by TTL domain, including alleles used and important features.

https://doi.org/10.1371/journal.pgen.1009052.g002

deletion of 137 AAs of the TTL domain (S2 Table), which is predicted to reduce or eliminate glutamylase function. As previously shown [21], *ttll-4(tm3310)* strongly suppressed the *ccpp-1* Dyf phenotype (Fig 2A).

The *ttll-5* gene also encodes two protein isoforms, TTLL-5A (677 AA) and TTLL-5B (730 AA) (Fig 2B; [29]). The TTL domain in TTLL-5 spans AA residues 67–425 in TTLL-5a and 120–478 in TTLL-5b. We characterized the recessive deletion allele *tm3360*, in which 49 AA are deleted, including 33 residues that align with the extended TTLL domain of mammalian TTLL5 [9,30]. Although this deletion is predicted to be in-frame, the large missing region of the TTLL domain might abolish or reduce substrate binding and glutamylase function [A. Roll-Mecak, personal communication]. *ttll-5(tm3360)* also strongly suppressed the *ccpp-1* Dyf phenotype in both amphids and phasmids (Fig 2A).

TTLL-11 also has two isoforms, TTLL-11A (607 AA) and TTLL-11B (707 AA) (Fig 2B; [29]). The TTL domain spans residues 24–388 in TTLL-11A and 124–488 in TTLL-11B. The *ttll-11(tm4059)* allele encodes an in-frame deletion in the TTL domain and is expected to disrupt function of both isoforms [22]. Like *ttll-4* and *ttll-5* mutations, *ttll-11(tm4059)* suppressed the *ccpp-1* Dyf phenotype in amphids and phasmids (Fig 2A). In contrast, *ttll-11b(gk482)*, which deletes coding sequence from only the long B isoform, did not suppress *ccpp-1*. We cannot completely rule out the possibility that *gk482* reduces expression of both TTLL-11A and TTLL-11B. However, transcriptional GFP reporters suggest that TTLL-11B is expressed in extracellular vesicle-releasing neurons (EVNs) and not amphids [31], whereas TTLL-11A may be expressed in amphids [22]. These data suggest that TTLL-11A opposes the activity of CCPP-1 in amphid and phasmid neurons.

We also tested candidate genes that are not predicted to act directly in opposition to CCPP-1 deglutamylase activity for a role in the suppression of ciliary degeneration due to loss of CCPP-1 function. Because *spas-1*/Spastin and *mei-1*/Katanin are implicated in the severing of glutamylated microtubules [32,33], we tested whether mutations in these genes altered *ccpp-1* hyperglutamylation-induced ciliary degeneration. Other candidates included the microtubule-depolymerizing kinesin-13 KLP-7 and the MAP kinase PMK-3, which interact with the deglutamylases CCPP-1 and CCPP-6 to regulate axon regrowth after laser-severing of *C. elegans* PLM touch receptor neurons [34]. Mutations in these and several other candidate genes failed to suppress the *ccpp-1* Dyf phenotype (S1 Fig), suggesting that other unidentified molecules modulate ciliary degeneration due to loss of CCPP-1 loss of function.

A forward genetic screen for suppressors of the *ccpp-1* dye-filling defect recovered alleles affecting the glutamylase TTLL-5 and the NIMA-related kinase NEKL-4

To identify genes that act with *ccpp-1* to regulate ciliary stability, we conducted a genetic screen for suppressors of the *ccpp-1(ok1821)* Dyf phenotype. We mutagenized >1000 P_0 *ccpp-1* mutants, passaged them to homozygose recessive mutations, performed dye-filling assays on F_2 adults, and screened for non-Dyf animals (Fig 3A). Mutant lines were maintained and retested for suppression of the Dyf phenotype. From >100,000 mutagenized haploid genomes, we isolated 11 viable lines that displayed suppression of the *ccpp-1* Dyf phenotype when retested (S1 Table).

The *my38* allele recovered in our screen suppressed the Dyf phenotype of *ccpp-1* in the amphid neurons in the head (Fig 2A; Fig 3B). We identified *my38* as a missense mutation in the *ttll-5* glutamylase gene. *my38* encodes an L338F substitution, located in the TTL domain (Fig 2B), that is predicted to affect ATP binding [A. Roll-Mecak, personal communication]. Therefore, our screen was able to identify a new allele of one of our candidate suppressor

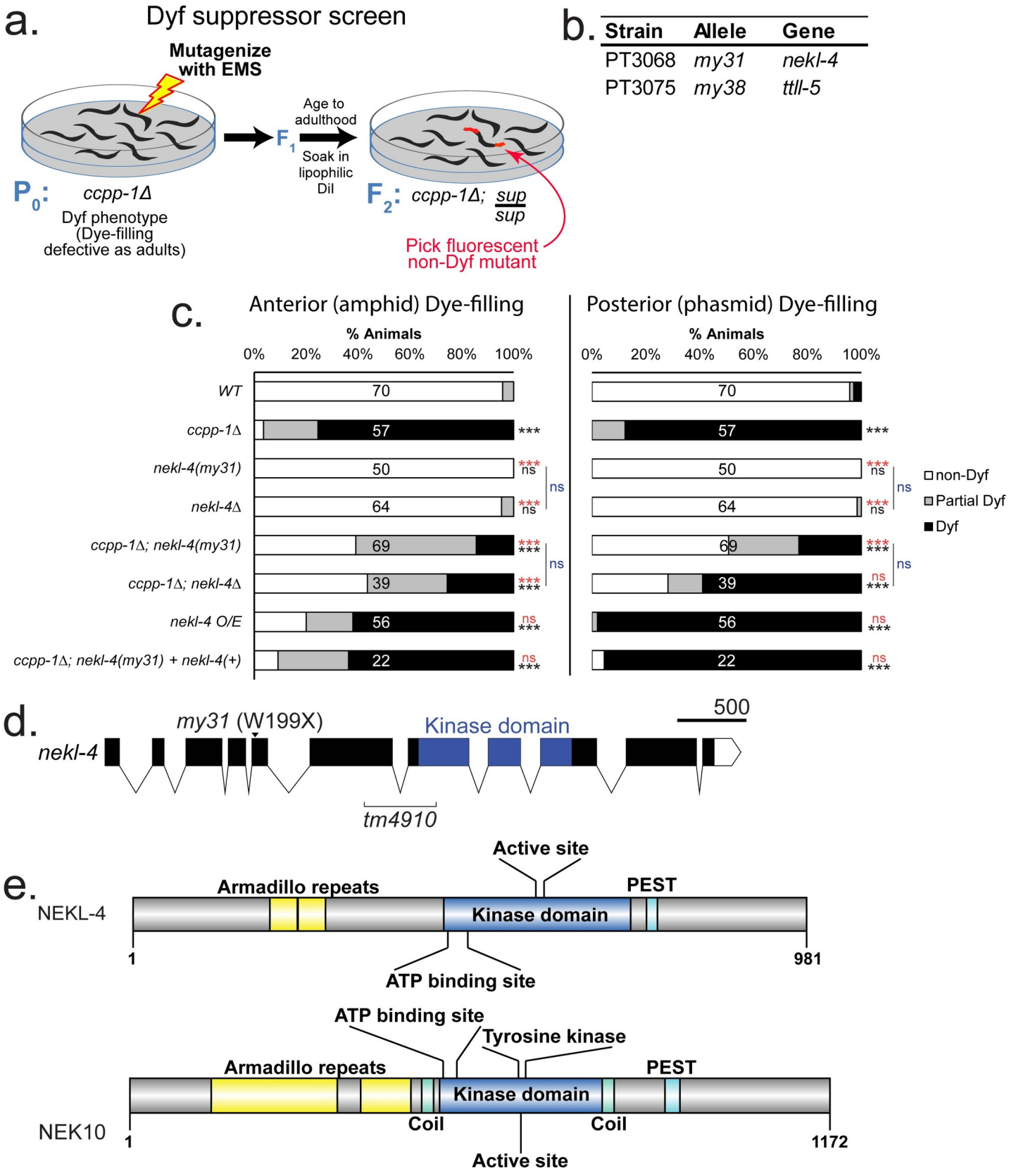
a.
Dyf suppressor screen
Mutagenize with EMS
P0: ccpp-1Δ
Dyf phenotype (Dye-filling defective as adults)
Age to adulthood
F1
Soak in lipophilic DiI
F2: ccpp-1Δ; sup/sup
Pick fluorescent non-Dyf mutant
b.
Strain Allele Gene
PT3068 my31 nekl-4
PT3075 my38 ttll-5
c.
Anterior (amphid) Dye-filling
Posterior (phasmid) Dye-filling
% Animals
0% 20% 40% 60% 80% 100%
WT
ccpp-1Δ
nekl-4(my31)
nekl-4Δ
ccpp-1Δ; nekl-4(my31)
ccpp-1Δ; nekl-4Δ
nekl-4 O/E
ccpp-1Δ; nekl-4(my31) + nekl-4(+)
70
57
50
64
69
39
56
22
***
ns
non-Dyf
Partial Dyf
Dyf
d.
nekl-4
my31 (W199X)
Kinase domain
500
tm4910
e.
NEKL-4
Armadillo repeats
Active site
PEST
Kinase domain
1
981
ATP binding site
NEK10
ATP binding site
Tyrosine kinase
Armadillo repeats
PEST
Kinase domain
Coil
Coil
1
1172
Active site

Fig 3. *ccpp-1* suppressor screen design and *ccpp-1* Dyf suppressors identified. a. Diagram of EMS mutagenesis screen for *ccpp-1* Dyf suppressors (*sup*). **b.** Outcrossed single-gene suppressors identified from mutagenesis screen and sequenced. Names of strains and alleles are indicated, as well as the genes identified through sequencing. **c.** Suppression of *ccpp-1* Dyf phenotype by *nekl-4*. N of animals per strain is indicated on bars. *** indicates $p \leq 0.0001$ by Kruskal-Wallis one-way ANOVA analysis and post hoc Dunn's multiple comparison test. Black indicates significance relative to wild type and red indicates significance relative to *ccpp-1Δ*. **d.** Diagram of *nekl-4* gene with alleles and important features indicated. **e.** Protein diagrams of NEKL-4 and its human homolog NEK10.

https://doi.org/10.1371/journal.pgen.1009052.g003

genes. This is important both as a validation of our screening method as well as a way to study the effects of different protein alterations on a phenotype.

Whole genome sequencing identified that our *my31* suppressor allele encodes a nonsense mutation in exon 5 of the *nekl-4* gene that produces NEKL-4(W199X) (**Fig 3B**; **S2 Table**; [29]). *nekl-4(my31)* moderately suppressed *ccpp-1* Dyf in both amphid and phasmid neurons and was non-Dyf as a single mutant (**Fig 3C**). *nekl-4* encodes a 981 AA putative serine-threonine kinase (**Fig 3D**). Prosite and InterPro scans detected a kinase domain (residues 453–725), and two armadillo (ARM) repeats (residues 200–281); ARM repeats are a series of alpha helices which can be indicative of protein-protein interactions [35]. Using EMBOSS epestfind [36], we also identified a PEST domain, important for proteolytic degradation (residues 748–764) [37]. NEKL-4 is a homolog of human NEK10, a protein required for ciliogenesis and associated with ciliopathies ([25,26]**;** **Fig 3E**). NEK10 also contains ARM repeats (residues 137–348 and 387–471), a kinase domain (residues 519–791), and a PEST domain (residues 896–921). However, the NEK10 kinase domain is flanked by coiled-coil domains and contains a putative tyrosine kinase active site not found in NEKL-4. NEKL-4 identity ranges from 29.41% (compared with NEK10 isoform 3) to 48.54% (NEK10 isoforms 5, 6 and 7). The NEK10 and NEKL-4 kinase domain is 52.50% identical by BLAST ([38]; **S2 Fig**).

To confirm that *my31* was a mutation in the *nekl-4* gene, we performed transgenic rescue experiments by germline injection of the wild-type genomic copy of *nekl-4* (injected @1.5ng/μL) into *ccpp-1;nekl-4(my31)* mutants, and restored the *ccpp-1* Dyf phenotype (**Fig 3C**). We also characterized the deletion allele *tm4910*, which removes portions of exon 6 and exon 7 and replaces part of the kinase domain, including the putative ATP-binding lysine residue, with a glutamine residue. *nekl-4(tm4910)* single mutants are non-Dyf. *nekl-4(my31)* and *nekl-4(tm4910)* exhibited similar suppression of *ccpp-1* Dyf defects in amphid and phasmid neurons. Because both alleles were phenotypically indistinguishable and are likely loss-of-function alleles, we continued with the *nekl-4(tm4910)* deletion allele for ease of genotyping.

NEKL-4 is expressed in ciliated neurons but does not localize to cilia

We examined NEKL-4 expression pattern and subcellular localization using an extrachromosomal *nekl-4p*::*nekl-4*::*gfp* reporter transgene and endogenously tagged *nekl-4*::*mneongreen* and *nekl-4*::*mscarlet* CRISPR reporters (**Fig 4A**). Extrachromosomal NEKL-4::GFP, driven by an endogenous promoter of 1609 base pairs before the start codon, localized in the axons, cell bodies, and dendrites of the ciliated neurons in the head of the worm, as well as the phasmid and PQR neurons in the tail, and was excluded from nuclei (**Fig 4B–4C**). NEKL-4::GFP localized to the distal dendrite and the base of sensory cilia, but was not observed in the cilium. In the dendrites of some neurons, NEKL-4::GFP accumulated in patches ranging from 2–5 μm in length. Overexpression of a *nekl-4p*::*nekl-4*::*gfp* transgene (injected at a concentration of 13 ng/μL) resulted in a Dyf phenotype (**Fig 3A**), suggesting that appropriate expression level or activity of NEKL-4 is important to ciliary stability.

We therefore examined the expression and localization of endogenous NEKL-4 by using CRISPR/Cas9 [39,40] to engineer *nekl-4*::*mneongreen* and *nekl-4*::*mscarlet* strains (**Fig 4D and 4E**). These CRISPR-generated reporters use the *nekl-4* locus as well as a short flexible linker, and have significantly dimmer fluorescence than the extrachromosomal *nekl-4p*::*nekl-4*::*gfp*

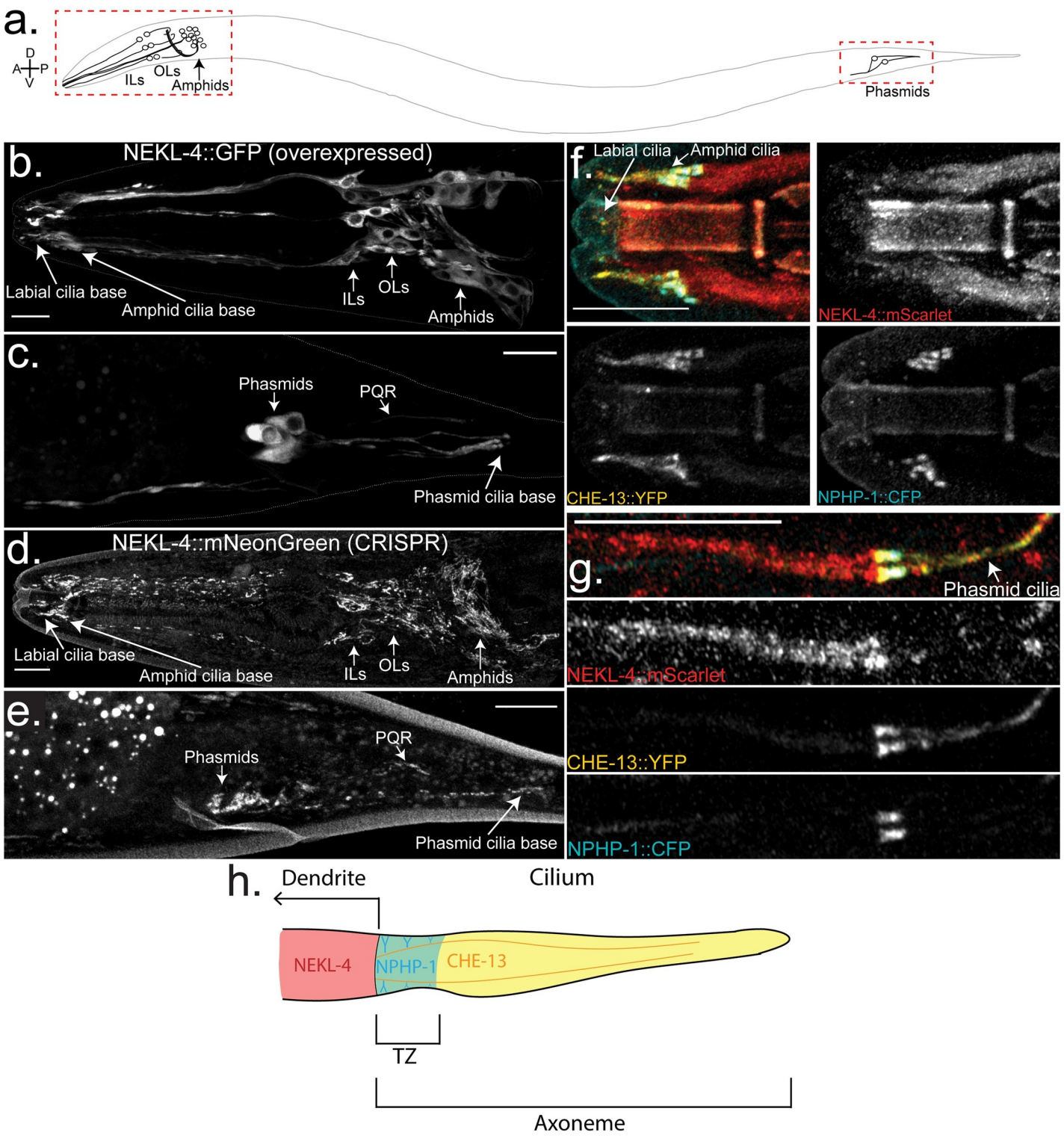

Fig 4. NEKL-4 is localized to ciliated neurons and is not enriched in the cilium. a. Diagram of a *C. elegans* hermaphrodite. Imaged areas are boxed. **b-c.** Localization of NEKL-4::GFP, overexpressed by an extrachromosomal array. Scale = 10μm. **d-e.** Localization of NEKL-4::mNeonGreen, expressed by inserting the fluorescent tag at the 3' end of the endogenous *nekl-4* gene using CRISPR/Cas9. Scale = 10μm. **f-g.** Localization of NEKL-4::mScarlet to the distal dendrite with NPHP-1::CFP (transition zone) and CHE-13::YFP (axoneme) as reference points. Scale = 10μm. **h.** Schematic of a phasmid cilium showing NEKL-4, NPHP-1, and CHE-13 localization.

https://doi.org/10.1371/journal.pgen.1009052.g004

array. With both extrachromosomal and CRISPR reporters, NEKL-4 was observed in the same neurons and similar subcellular locations.

With the CRISPR-generated *nekl-4*::*mneongreen* reporter, we were able to resolve fine structures in the cell bodies and dendrites. In the amphid cell bodies, NEKL-4::mNG appeared as thin filaments. A similar pattern was seen in the outer labial (OL), inner labial (IL), and cephalic (CEP) cell bodies, though the filaments appeared to be thicker and brighter. The CRISPR-generated NEKL-4::mNG reporter also localized in discrete, discontinuous patches in the dendrites. This pattern continued to the distal dendrite, terminating before entering the cilium of any neurons. We observed NEKL-4::mNG movement in the distal dendrite (**Movie S1**) and localization to the cell bodies and dendrites of the ray neurons in the male tail (**S3 Fig**). The intricate localization pattern and movement of NEKL-4::mNG suggests association with organelles or cytoskeletal components.

Because a *nekl-4*::*gfp* reporter was previously reported [41] to localize in phasmid cilia, we examined colocalization of NEKL-4::mScarlet with CHE-13/IFT57, an IFT-B component [42], and NPHP-1, a transition zone protein, to confirm NEKL-4 exclusion from the cilium. NEKL-4::mSC did not show significant overlap with NPHP-1::CFP or CHE-13::YFP, and was mainly restricted to the distal dendrite and periciliary membrane compartment (PCMC) (**Fig 4F and 4G**). We hypothesize that the discrepancy between our results and those of Yi *et al* [41] regarding NEKL-4 localization could be due to the higher injection concentration of their construct (50ng/μL vs. 13ng/μL for our extrachromosomal reporter), and the use of the *dyf-1* promoter as opposed to the endogenous *nekl-4* promoter that we utilized for both our extrachromosomal reporter and CRISPR markers. From our data, we conclude that NEKL-4 functions in ciliated neurons, although the protein itself does not localize to the cilium (**Fig 4H**).

ttll-4(tm3310) and *ttll-5(tm3360)* partially suppress *ccpp-1* glutamylation defects. *ttll-11* activity is essential for glutamylation but not ciliogenesis

To analyze the effect of our suppressor mutations on microtubule glutamylation, we conducted indirect immunofluorescence experiments. We used the monoclonal antibody GT335, which recognizes the branch point of glutamate side-chains [43]. In wild type, GT335 labels the cilia of amphid, labial (OL, IL), and cephalic (CEP) neurons (**Fig 5A**; **S4 Fig**). Labial and cephalic cilia are seen at the anterior-most tip of the animal, surrounding the buccal cavity. GT335 staining of labial and cephalic cilia appeared as singular axonemes [44]. In amphid channel cilia, GT335 specifically stains the doublet region middle segments that appear as two triangular bundles located posterior to the labial and cephalic cilia [44]. In wild type animals, GT335 strongly stained labial and cephalic cilia and amphid ciliary middle segments (**Fig 5B**). In the *ttll-4(tm3310)* mutants, we observed a reduction in the percentage of animals with amphid, labial and cephalic staining with GT335, indicating that mutations in TTLL-4 affect glutamylation (**Fig 5C**). In the *ttll-5(my38)* and *ttll-5(tm3360)* single mutants, we observed normal GT335 staining (**Fig 5C**). The *ttll-11(tm4059)* mutation, which affects both TTLL-11 isoforms, abolished GT335 staining, whereas *ttll-11b(gk482)* showed normal GT335 staining in amphid middle segments (**Fig 5B and 5C**).

We next examined the effect of the *ttll* gene suppressor mutations on GT335 staining in the *ccpp-1* mutant background. We analyzed both the presence of GT335 staining and the appearance of staining to examine subtle differences in glutamylation patterns. We observed a variation in the GT335 staining pattern of some mutants: the amphids were stained but the pattern was abnormal. We classified this staining pattern as an "abnormal amphid" phenotype (**Fig 5B**). We observed abnormal phenotypes in ciliary glutamylation in *ttll* mutants and suppressor strains. In some mutants, including *ccpp-1*, labial and cephalic cilia stained, while amphid cilia

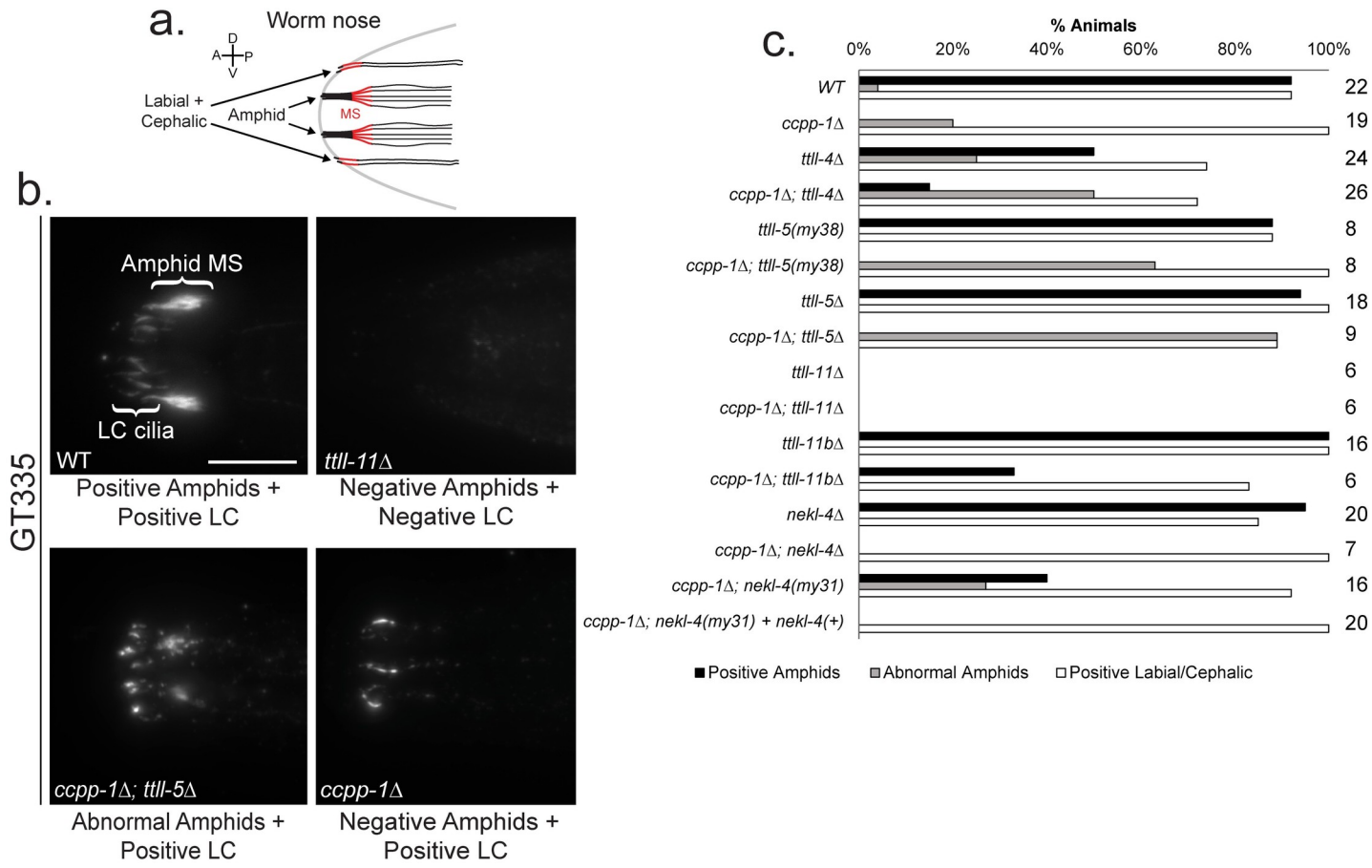

Fig 5. Effects of mutations on glutamylation of amphid, labial and cephalic (LC) cilia. a. Diagram of the cilia of the *C. elegans* nose. Red indicates areas that are strained by the GT335 antibody, indicating glutamylation (adapted from *O'Hagan et al* [22]). MS = amphid middle segments; LC = labial and cephalic cilia. **b.** Examples of GT335 antibody staining phenotypes. Scale = 10μm. **c.** Percentage of worms with GT335 stained amphids and/or LC cilia. *ccpp-1Δ; nekl-4(my31)* was rescued with a *nekl-4p*::*nekl-4*::*gfp* plasmid @ 1.5ng/μL. N of animals per strain is indicated.

https://doi.org/10.1371/journal.pgen.1009052.g005

did not, consistent with cell-specific regulation of the Tubulin Code [2,22,34,45] (Fig 5B). In *ccpp-1* mutant amphid channel cilia, GT335 staining was often undetectable, and occasionally detectable but abnormal (Fig 5B). We observed some restoration of GT335 staining in ampid channel cilia in 15% of the *ccpp-1;ttll-4* double mutant animals (Fig 5C). In *ccpp-1;ttll-5* double mutants, we observed a higher incidence of abnormal amphid middle segments compared to the *ccpp-1* single mutant (Fig 5C). In the *ccpp-1;ttll-11(tm4059)* double mutants, GT335 staining was undetectable (Fig 5C). *ccpp-1;ttll-11b(gk482)* mutants, in contrast, had some restoration of amphid and labial and cephalic GT335 staining (Fig 5C).

We also used a polyE antibody, which detects side-chains of 3 or more glutamates [5]. PolyE staining of wild-type males strongly labelled amphid middle segments and labial cilia, suggesting that microtubules in these cilia are decorated with side chains of at least 3 glutamates. Mutations in *ttll-4* and *ttll-5* did not detectably reduce polyE staining. The *ttll-11 (tm4059)* mutation, however, abolished polyE staining (S5 Fig). Our results on the effect of the suppressor mutations on polyE staining in *ccpp-1* mutants closely matched our observations with GT335. In *ccpp-1* mutants, amphid channel cilia polyE staining was rarely observed (in 10% of animals) and more often appeared abnormal (S5 Fig). In *ccpp-1;ttll-5(tm3360)* and *ccpp-1;ttll-11b(gk482)* double mutant animals, we observed increases in the incidence of polyE

stained amphid cilia (S5 Fig). We note that the absence of GT335 and polyE staining indicates an absence of glutamylation, but not necessarily an absence of MTs. Taking into account our antibody staining results, Dyf phenotype suppression, and previously published transmission electron microscopy data [21], we propose that our data indicates that loss of microtubule glutamylase activity suppresses microtubule degeneration due to loss of CCPP-1 function, and that microtubule glutamylation is not essential for dye filling or ciliogenesis. Overall, our data suggests that TTLL-11 is essential for adding the initiating "branch point" glutamate and that TTLL-4 and TTLL-5 are not essential for initiating glutamate side-chains. TTLL-4 and TTLL-5 might act primarily as elongases, but loss of their function was not sufficient to reduce the chain length to less than 3 glutamates.

nekl-4(my31), but not *nekl-4(tm4910)*, mildly suppresses *ccpp-1* glutamylation defects

We also examined whether NEKL-4 affects microtubule glutamylation. *nekl-4(tm4910)* did not affect GT335 staining, indicating NEKL-4 is not essential for initiating glutamate side-chains (Fig 5C). Unlike *ttll-4* and *ttll-5* mutations, *nekl-4(tm4910)* did not suppress the abnormal GT335 staining in *ccpp-1*. Curiously, although *nekl-4(my31)* and *nekl-4(tm4910)* phenocopied each other in *ccpp-1* Dyf suppression, their effects on *ccpp-1* GT335 phenotype were different, in that *nekl-4(my31)* showed a partial suppression of the *ccpp-1* GT335 phenotype (Fig 5C). *nekl-4(my31)* also mildly suppressed the *ccpp-1* polyE phenotype (S5 Fig). In transgenic animals, introduction of a *nekl-4(+)* genomic construct rescued *ccpp-1;nekl-4(my31)* amphid GT335 staining to appear similar to *ccpp-1* alone (Fig 5C). Based on our antibody staining data, we conclude that NEKL-4 may act downstream or independent of CCPP-1-mediated deglutamylation.

ttll-5 and *ttll-11* suppress heterotrimeric kinesin-II span shortening in *ccpp-1* mutants

C. elegans amphid and phasmid cilia are built by the cooperative action of heterotrimeric kinesin-II and homodimeric OSM-3/KIF17 [46,47]. Heterotrimeric kinesin-II travels along the doublet-containing middle segment region, which makes up approximately half of the length of the amphid channel and phasmid cilia and correlates with GT335 staining ([46,47]; Fig 6A). We therefore examined the middle segment localization of KAP-1::GFP, the non-motor subunit of heterotrimeric kinesin-II ([46]; Fig 6B). In wild-type phasmid cilia, the span of KAP-1::GFP was approximately 4μm (Fig 6C). In *osm-3(p802)* mutants that lack distal singlet microtubules, we observed a similarly reduced KAP-1::GFP span of 2μm [18,20,44]. In *ccpp-1* mutants, the KAP-1::GFP span was significantly reduced to approximately 2μm. We considered the following possibilities to explain the shortened KAP-1::GFP span in *ccpp-1*: (i) microtubule loss in *ccpp-1* mutants, or (ii) altered association with OSM-3 in the 'handover zone', which may be needed for heterotrimeric kinesin-II to travel the appropriate distance [48]. Both of these possibilities are consistent with roles for the Tubulin Code in regulating microtubule stability and motor properties. To further understand the mechanism of suppression of the *ccpp-1* Dyf phenotype, we examined KAP-1::GFP spans in suppressor mutations in wild type and *ccpp-1* backgrounds. KAP-1::GFP spans were similar to wild type in *ttll-4*, *ttll-5*, *ttll-11*, and *nekl-4 (tm4910)* single mutants suggesting that the single mutants alone did not not cause microtubule loss, or affect kinesin-II interactions with OSM-3 (Fig 6C). The former conclusion is consistent with a lack of Dyf phenotypes in *ttll-4*, *ttll-5*, *ttll-11*, and *nekl-4(tm4910)* mutants. Mutations in *ttll-5* and *ttll-11* that suppressed the Dyf phenotype of *ccpp-1* also suppressed the KAP-1::GFP span shortening of *ccpp-1* (Fig 6C). Importantly, suppression of KAP-1::GFP

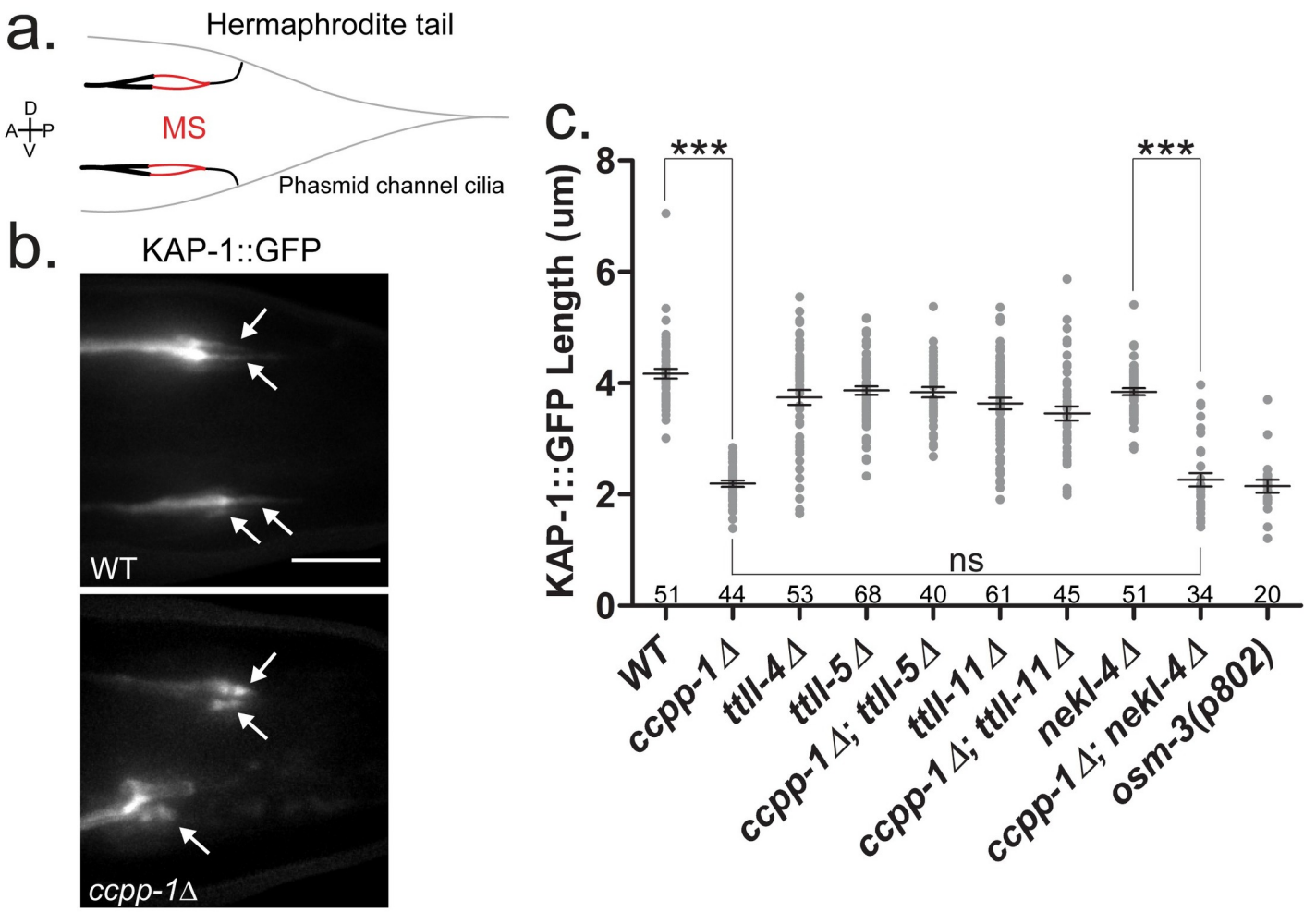
a.
Hermaphrodite tail
D
A
P
V
MS
Phasmid channel cilia
b.
KAP-1::GFP
WT
ccpp-1Δ
c.
KAP-1::GFP Length (um)
***
***
ns
51 44 53 68 40 61 45 51 34 20
WT
ccpp-1Δ
ttll-4Δ
ttll-5Δ
ccpp-1Δ; ttll-5Δ
ttll-11Δ
ccpp-1Δ; ttll-11Δ
nekl-4Δ
ccpp-1Δ; nekl-4Δ
osm-3(p802)
d.
Anterior (amphid) Dye-filling
Posterior (phasmid) Dye-filling
% Animals
0% 20% 40% 60% 80% 100%
WT 50 50
osm-3(p802) 33 32
ttll-4Δ 50 50
ttll-4Δ; osm-3(p802) 20 20
ttll-5Δ 27 27
osm-3(p802); ttll-5Δ 50 50
ttll-11Δ 50 50
osm-3(p802); ttll-11Δ 25 25
nekl-4Δ 37 37
nekl-4Δ; osm-3(p802) 32 32
non-Dyf
Partial Dyf
Dyf

Fig 6. Mutations in TTLL genes suppress *ccpp-1* defects in KAP-1 middle segment localization, but do not suppress distal segment defects in *osm-3(p802)* mutants. a. Diagram of the *C. elegans* hermaphrodite phasmid cilia. MS = phasmid middle segments. **b.** Examples of KAP-1::GFP localization in the phasmid cilia. Arrows = individual phasmid cilia. Scale = 5μm. **c.** Length of KAP-1::GFP span in the phasmid neurons. Mean ± SEM. *** indicates $p \leq 0.0001$ by Kruskal-Wallis one-way ANOVA analysis and post hoc Dunn's multiple comparison test. n of cilia per strain is indicated. **d.** Dye-filling assay showing lack of *osm-3(p802)* suppression by *ttll-4*, *ttll-5*, *ttll-11* or *nekl-4*. N of animals per strain is indicated.

https://doi.org/10.1371/journal.pgen.1009052.g006

span shortening of *ccpp-1* by *ttll-11* confirmed the presence of ciliary MTs despite the lack of antibody staining in *ccpp-1;ttll-11(tm4059)* double mutants. *nekl-4(tm4910)* did not suppress the *ccpp-1* KAP-1::GFP span shortening (**Fig 6C**). Our data suggests that reduction of microtubule glutamylation rescues ciliary degeneration caused due to CCPP-1 loss of function by suppressing ciliary microtubule loss, altering motor protein-IFT particle interactions, or both. Additionally, our data on *nekl-4(tm4910)* revealed the presence of a mechanism for *ccpp-1* Dyf suppression that does not involve detectable changes in microtubule glutamylation or heterotrimeric kinesin-II location.

In addition to heterotrimeric kinesin-II, homodimeric OSM-3/KIF17 kinesin-2 is important for ciliogenesis in amphid and phasmid neurons [18,49,50]. A previous study indicated that *nekl-4* genetically interacts with *osm-3* [41]. *nekl-4(cas396)*, which affects the kinase domain, partially suppresses the Dyf phenotype and distal segment loss of *osm-3(sa125)* mutants [41]. The *osm-3(sa125)* G444E missense mutation is proposed to relieve the autoinhibition of the coiled-coil stalk of OSM-3 by fixing its hinge region in an extended conformation, but severely impairs its motility. OSM-3(G444E) can still associate with heterotrimeric kinesin-II [41,50]. We examined genetic interactions between the *nekl-4(tm4910)* deletion allele and the *osm-3(p802)* allele, which phenocopies the *osm-3(sa125)* amphid cilia truncation phenotype [18,41]. The *osm-3(p802)* null mutation was not suppressed by *nekl-4(tm4910)*, indicating that interactions between *nekl-4* and *osm-3* are allele-specific, and may depend on the physical or functional interactions between OSM-3 and NEKL-4 (**Fig 6D**).

Discussion

We used a forward genetic screen and candidate approach to identify genes that act with the *ccpp-1* deglutamylase to control ciliary stability. We identified tubulin code writers and effectors of ciliary stability as modulators of degenerative phenotypes associated with CCPP-1 loss. Our data provides insight into how glutamylation is precisely controlled to maintain ciliary structure and function and to prevent neurodegeneration. Ciliary degeneration in *ccpp-1* mutants can be suppressed by altering microtubule glutamylation through the loss of function of tubulin glutamylating enzymes TTLL-4, TTLL-5, or TTLL-11 (refer to model in **Fig 7**). Our findings are in agreement with studies in *Chlamydomonas*, where reducing microtubule glutamylation has a stabilizing effect on axonemal defective mutants ([51,52]; for a summary of phenotypes, refer to **S3 Table**).

Loss of the NIMA related kinase NEKL-4 opposes the *ccpp-1* effect on ciliary stability and may act independently of microtubule glutamylation state. Loss of NEKL-4 function suppresses the *ccpp-1* Dyf phenotype while animals overexpressing NEKL-4::GFP are Dyf. Our findings are consistent with previous reports on the roles of NIMA kinases in regulating axonemal stability [52–54]. *nekl-4(tm4910)* does not strongly affect GT335 staining, arguing against a role for NEKL-4 in the regulation of a glutamylase or deglutamylase enzyme, although we cannot completely rule out this possibility. NEKL-4 is also unlikely to be a reader of ciliary glutamylation because it is largely absent from cilia. Future studies should prioritize ultrastructural analysis by performing transmission electron microscopy to characterize the effect of suppressor mutations on ciliary microtubule loss in *ccpp-1* mutants.

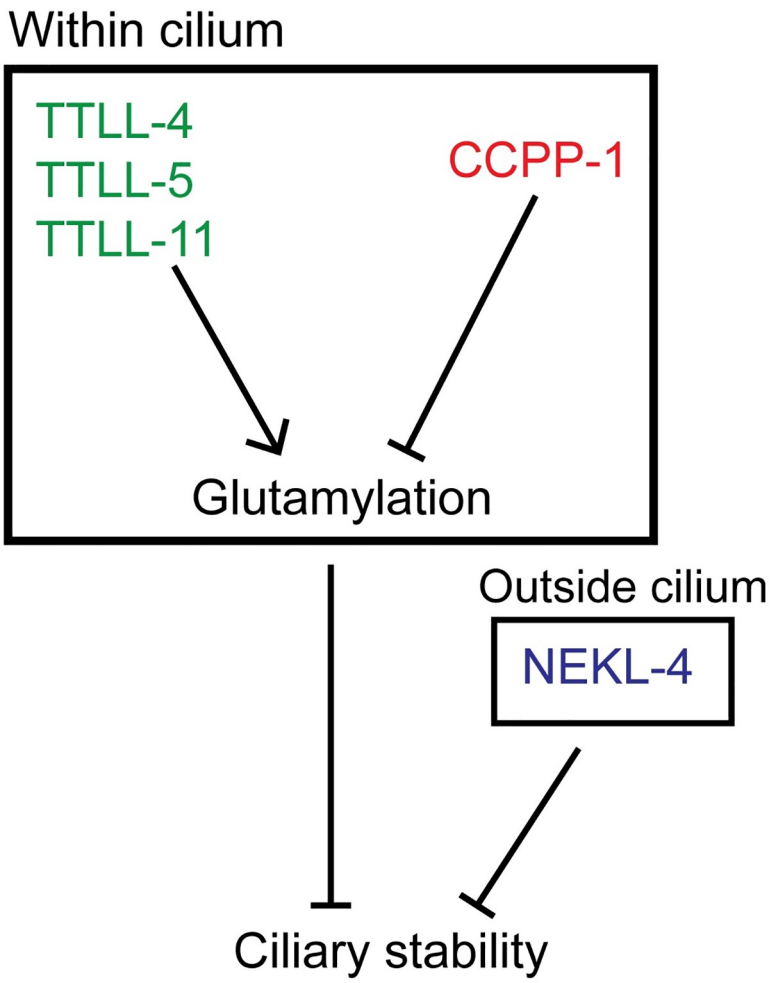

Fig 7. Schematic of TTLL-4, TTLL-5, TTLL-11, CCPP-1, and NEKL-4 interactions and effects on ciliary stability.

https://doi.org/10.1371/journal.pgen.1009052.g007

How does NEKL-4 regulate ciliary stability despite not localizing to cilia? Several processes including IFT loading/unloading, flagellar length sensing, and ciliary entry of proteins depend on the phosphorylation state of kinesin-II and other IFT components at the base of the cilium [55–58]. Potential substrates of the NEKL-4 human homolog NEK10 include kinesins, IFT components, and other ciliary proteins that have homologs in *C. elegans* ([26,59]**; S4 Table**). In human bronchial epithelial cell (HBEC) culture, NEK10 mutation caused a reduction in phosphopeptides of gene products including KIF13B, KIF19, IFT140, IFT46, IFT88, and MAK [26]. These genes and their *C. elegans* orthologs *klp-4*, *klp-13*, *che-11*, *dyf-6*, *osm-5*, and *dyf-5* are involved with microtubule dynamics, IFT, and ciliary structure [41,60–68]. NEKL-4 may function in the distal dendrite or periciliary membrane compartment to phosphorylate IFT-related proteins before ciliary entry to indirectly modulate IFT.

NEKs may also regulate endocytosis. *C. elegans* NEKL-2 and NEKL-3 control clathrin-mediated endocytosis and trafficking in non-ciliated cells [69–71]. NEKL-4 localizes to the periciliary membrane compartment, an active site of endocytosis, a process necessary for regulating ciliary membrane volume, ciliary protein levels, and IFT [72]. Consistent with this idea, a reduction in endocytosis can rescue the Dyf defect of a dominant active G protein α subunit (*gpa-3QL*) mutant [73].

What could be the mechanism by which loss of CCPP-1 results in ciliary instability? Our data argue against a role for microtubule severing by katanin (MEI-1) and spastin (SPAS-1) in modulating the loss of ciliary stability in *ccpp-1* mutants. Our results also did not support a role for other known effectors of microtubule glutamylation—the MAP kinase PMK-3 and the microtubule-depolymerizing kinesin-13 (KLP-7), in the degradation of ciliary microtubules in the absence of CCPP-1 function. Previous studies in *Chlamydomonas* revealed a link between tubulin turnover and both tubulin polyglutamylation [74] and NEK kinase activity [52]. Changes in IFT due to loss of CCPP-1 function could affect tubulin transport [75], or the binding of structural MAPs [76,77] could also mediate *ccpp-1* loss induced loss of ciliary stability. Identification of readers of the tubulin code in amphid and phasmid neurons could identify molecules and mechanisms that modulate ciliary degeneration in response to changes in microtubule glutamylation.

NIMA-related kinases play major roles in microtubule structure regulation and processes such as mitosis, ciliogenesis, and post-translational modifications [54,78–80]. Consequently, mutations of NEKs may result in cancer [81–83] and ciliopathies, such as polycystic kidney disease [26,80,84]. Many NEKs regulate ciliary disassembly through promotion of microtubule instability, such as *Tetrahymena* Nrk2, Nrk17, and Nrk30 [54], *Chlamydomonas* FA2, CNK2, and CNK11 [52,85,86], and human NEK7 [53]. Our data on the effects of NEKL-4 on ciliary stability offers insight into mucociliary disease associated with mutations in human NEK10. Our data also expands upon an evolutionarily-conserved link between molecules involved in microtubule glutamylation and NEK kinases [52,87]. Our studies provide a model for the exploration of this poorly-understood link between NEK kinases and microtubule glutamylation, and identify NEKs as a modulator of the degenerative effects associated with dysregulated levels of microtubule glutamylation. The data shown in this work will inform future studies on neurodegenerative disorders and ciliopathies associated with mutations in microtubule glutamylation enzymes and NEK kinases.

Materials and methods

C. elegans strains and maintenance

Nematodes were cultured on Nematode Growth Media (NGM) agar plates containing a lawn of OP50 *E. coli* and incubated at 20˚C, as previously described [88]. Strains used are listed in **S5 Table**. Some strains contained *him-5(e1490)* and/or *myIs1[pkd-2*::*gfp+unc-122p*::*gfp] pkd-2 (sy606)*, which were considered wild type.

ccpp-1 EMS mutagenesis screen

To identify the pathway by which *ccpp-1* mutations cause the Dyf phenotype [21], we performed a forward genetic screen for suppressors of the Dyf defect of *ccpp-1* mutants. Ethyl methanesulfonate (EMS; Sigma Aldrich Cat. M0880) was used to mutagenize *ccpp-1(ok1821)* mutants {either Strain PT2168—*ccpp-1(ok1821);myIs1[pkd-2*::*gfp + unc-122p*::*gfp] pkd-2 (sy606);him-5(e1490)* or OE4160—*ccpp-1(ok1821)*}. L4 larvae were suspended in 1 ml of M9 buffer [89] with a final concentration of 47 mM EMS for four hours, before washing three times in M9 and depositing worm suspension onto an NGM plate seeded with OP50 *E. coli* to recover. We then transferred 10 or 20 of these mutagenized P_0 hermaphrodites to new NGM plates and allowed them to lay eggs on 100mm NGM plates seeded with OP50 for one day or two days before removing them. When the F_1 hermaphrodites reached adulthood, we synchronized the age of F_2 progeny by hypochlorite treatment of gravid adult F_1 animals [89] and replating embryos on NGM plates with OP50. We then incubated plates for four days at 20˚C or five days at 15˚C (to allow the age-synchronized F_2 progeny to reach adulthood) before

washing them off plates using M9 to be dye-filled using the method described below. *ccpp-1* mutants without suppressor mutations typically are completely Dye-filling defective (Dyf) by adulthood. Therefore, to isolate suppressor mutants, we picked F_2 adult animals that were non-Dyf or incompletely Dyf. We isolated up to five suppressor mutant isolates corresponding to a single P_0 plate to allow for some lethality, but in most cases kept only a single suppressor from each P_0 plate, except as noted in **S1 Table**.

In total, we examined more than 100,000 haploid genomes. We isolated 93 non-Dyf or partially Dyf F_2 animals, of which 79 either died, were sterile, or were Dyf (not suppressed) in a subsequent secondary dye-filling assays to confirm the phenotype. 14 isolates were viable and produced non-Dyf or partial Dyf progeny in secondary screens, of which we consider 11 to be independent isolates. **S1 Table** is based on the qualitative analysis where amphid and phasmid neurons were not scored separately.

Whole-genome sequencing

To facilitate identification of suppressor mutations, whole-genome sequencing (WGS) was performed using the strategy described in Doitsidou *et al* [90]. Mutants were crossed with PT3037, a strain in which *ccpp-1* had been introgressed into the Hawaiian wild isolate genomic background by backcrossing ten times into CB4856. From crosses of PT3068 (*my31*) X PT3037, at least 20 suppressed F_2s were isolated; these F_2s were pooled for WGS to identify genomic intervals that lacked PT3037-derived single-nucleotide polymorphisms (SNPs); novel SNPs within those intervals potentially represent the suppressor mutation.

Adapter-ligated libraries were prepared from genomic DNA using the manufacturer's protocol (Illumina, San Diego, CA) from PT3037 and the pooled suppressed F_2s. A HiSeq 2000 instrument (Illumina, San Diego, CA) was used to sequence the genomic libraries. To identify the *my31* mutation, we used a pipeline described in Wang *et al* [91]. Briefly, the pipeline was as follows: BFAST for alignment [92], SAMtools for variant calling [93], and ANNOVAR for annotation [94]. We compared sequence data with *C. elegans* genome version WS220 to identify mutations. To identify mapping intervals that might contain the *my31* suppressor, we plotted Hawaiian SNP density against chromosome position. Non-Hawaiian SNPs that were also identified in PT3037 were removed as background. Candidate mutations for *my31* were identified as novel homozygous non-synomymous coding variants within the mapping interval.

To facilitate identification of suppressor mutations, mutants were crossed with PT3037 (a strain in which *ccpp-1* had been introgressed into the Hawaiian wild isolate genomic background by backcrossing ten times into CB4856). From crosses of PT3068 (*my31*) X PT3037, at least 20 suppressed F_2s were isolated; these F_2s were pooled for whole genome sequencing using the strategy described in Doitsidou *et al* [90] to identify genomic intervals containing N2 single nucleotide polymorphisms (SNPs) as potentially containing the suppressor mutation.

Adapter-ligated libraries were prepared from genomic DNA using the manufacturer's protocol (Illumina, San Diego, CA) from PT3037 and the pooled suppressed F_2s. A HiSeq 2000 instrument (Illumina, San Diego, CA) was used to sequence the genomic libraries. To identify the *my31* mutation, we used a pipeline described in Huang et al [95]. Briefly, the pipeline was as follows: BFAST for alignment [92], SAMtools for variant calling [93], and ANNOVAR for annotation [94]. We compared sequence data with *C. elegans* genome version WS220 to identify mutations. To identify N2 intervals that might contain the *my31* suppressor, we plotted Hawaiian SNP density against chromosome position. Non-Hawaiian SNPs that were also identified in PT3037 were removed as background.

Protein domain identification, homology analysis and alignments

Sequences of *ttll-4*, *ttll-5*, *ttll-11*, and *nekl-4* were obtained from WormBase [29] and protein sequences were obtained from WormBase or UniProt [96]. Structural predictions and protein domain information were generated with InterPro [97] and ScanProsite [98]. The PEST proteolytic degradation site in NEKL-4 was identified using EMBOSS epestfind [36]. NEKL-4 homology to NEK10 was predicted using protein BLAST [99] and human NEK10 and *C. elegans* NEKL-4 kinase domains were aligned using T-COFFEE Expresso [30]. All scans and queries described above were performed using default settings. Gene diagrams were created with the WormWeb Exon-Intron graphic maker [100], and protein diagrams were created with DOG 2.0 software [101,102]. The NEK10/NEKL-4 kinase domain alignment figure was generated with BoxShade [103] from the T-COFFEE sequence alignment.

Dye-filling assays

Three days prior to performing dye-filling assays, healthy, non-crowded plates containing many gravid hermaphrodite animals were washed and bleached to synchronize the worms. Day 1 and Day 2 adults were washed from the plate with 1mL M9 buffer and transferred to 1.5mL tubes. A stock solution of 2.5mg/mL DiI (Thermo Fisher Cat. D282) was added to a 1:1000 dilution and worms were incubated with gentle shaking for 30 min at room temperature. Prior to scoring, worms were briefly spun at 2000RPM and plated on new seeded NGM plates for approximately 1hr to excrete excess dye. The presence and intensity of dye in the amphid and phasmid neurons was visually scored using a dissecting microscope. Worms scored as non-Dyf were similar in brightness to wild type, and Dyf worms had no staining. Partial Dyf worms had dye present, but distinguishably less bright than wild type. Kruskal-Wallis one-way ANOVA analysis (where non-Dyf = 2, partial Dyf = 1. and Dyf = 0) and posthoc Dunn's multiple comparison test were performed in Prism (Graphpad Software).

Antibody staining

We performed immunofluorescence microscopy using the protocol described in O'Hagan *et al* [22]. We synchronized animals by bleaching and fixed as Day 1 adults. Fixation was accomplished by washing animals from 3 NGM plates using M9 buffer, then washing animals in a 15 ml conical tube 3 more times with M9 over one hour. Worms were chilled on ice before washing in ice-cold Ruvkun buffer (80 mM KCl, 20 mM NaCl, 10 mM EGTA, 5 mM spermidine-HCl, 15 mM Pipes, pH 7.4 and 25% methanol) plus 2% formaldehyde in 1.5ml centrifuge tubes. The tubes were immersed in liquid nitrogen and melted under tap water to crack the worms' cuticles. Worms were then washed twice with Tris-Triton buffer (100 mM Tris-HCl, pH 7.4, 1% Triton X-100 and 1 mM EDTA), suspended in Tris-Triton buffer+1% β-mercaptoethanol, and incubated overnight at 37˚C. The next day, worms were washed with 1X BO_3 buffer (50 mM H_3BO_3, 25 mM NaOH) + 0.01% Triton, and suspended in 1X BO_3 + 0.01% Triton buffer + 10 mM DTT for 15 minutes with gentle agitation at room temperature. Worms were then washed with 1X BO_3 buffer (50 mM H_3BO_3, 25 mM NaOH) + 0.01% Triton, and suspended in 1X BO_3 + 0.01% Triton buffer + 0.3% H_2O_2 for 15 minutes with gentle agitation at room temperature. After washing once with 1X BO_3 + 0.01% Triton buffer, worms were washed for 15 minutes in Antibody buffer B (1X PBS, 0.1% BSA, 0.5% Triton X-100, 0.05% sodium azide, 1mM EDTA) with gentle agitation at room temperature. Fixed worms were stored in Antibody buffer A (1X PBS, 1% BSA, 0.5% Triton X-100, 0.05% sodium azide, 1mM EDTA) at 4˚C for up to one month before antibody staining. Animals were stained overnight at room temperature with a 1:450 dilution (in Antibody Buffer A) of GT335 (Adipogen Cat.

AG-20B-0020-C100), a monoclonal antibody which binds the branch point of both monoglutamylated and polyglutamylated substrates [43], or polyE (Adipogen Cat. AG-25B-0030-C050), a polyclonal antibody which only binds polyglutamylated substrates (3 or more glutamate residues) [5]. Stained worms were washed with several changes of Antibody B Buffer with gentle agitation at room temperature over several hours. After rinsing with Antibody Buffer A, Alexa-fluor 568-conjugated donkey anti-mouse secondary antibody (Invitrogen Cat. A10037) was added at a final dilution of 1:2500 and incubated for 2 hours at room temperature with gentle agitation. Worms were then washed with several changes of Antibody Buffer B over several hours before mounting on 2% agarose pads for imaging.

We observed variation between and within individual GT335 staining experiments with respect to pattern and intensity. Environmental factors may cause changes in levels of ciliary glutamylation as measured by GT335 intensity [104]. It is therefore possible that small variations in experimental techniques or day-to-day lab conditions could have impacted our results. However, the GT335 staining phenotype of each mutant was generally consistent across trials.

Confocal imaging

Day 1 adult hermaphrodites were anaesthetized with 10 mM levamisole and mounted on 4% agarose pads for imaging at room temperature. Confocal imaging was performed with a Zeiss LSM 880 inverted microscope with an Airyscan superresolution module using a LSM T-PMT detector and ZenBlack software (Carl Zeiss Microscopy, Oberkochen, Germany). Laser intensity was adjusted to avoid saturated pixels. Images were acquired using a 63x/1.4 Oil Plan-Apochromat objective in Airyscan Fast mode and deconvolved using Airyscan processing. Image files were imported into Fiji/ImageJ [105] with the BioFormats Importer plugin for linear adjustment of contrast and creation of maximum intensity projections, and Adobe Photoshop CS5 was used to trace the outlines of the worm if needed. Images were placed in Adobe Illustrator CS5 for figure assembly.

KAP-1::GFP localization analysis

Nematodes were mounted as above. Widefield images were acquired on a Zeiss Axio Observer with Colibri 7 LEDs and ZenBlue software (Carl Zeiss Microscopy, Oberkochen, Germany) using a Photometrics Prime 95B sCMOS camera (Teledyne Photometrics, Tucson, AZ). A 100x/1.4 Oil Plan-Apochromat objective was used for imaging the phasmid cilia of Day 1 hermaphrodite animals. Images were imported into Fiji/ImageJ [105] and the length of KAP-1::GFP labeling was measured for each cilium using maximum intensity projections. Length was measured starting at the transition zone, which is distinct and bright, and ending when fluorescence was no longer visible. Kruskal-Wallis one-way ANOVA analysis and posthoc Dunn's multiple comparison test were performed in Prism (Graphpad Software).

We also wanted to examine if *ttll-4* suppressed the *ccpp-1* KAP-1::GFP span defect, but were unable to obtain a viable *ccpp-1;ttll-4;Ex[kap-1*::*gfp +pRF4]* strain, possibly due to synthetic lethality with the overexpressed *kap-1*::*gfp* reporter.

Plasmid construction

For creation of pRO139 (*nekl-4p*::*nekl-4*::*gfp*), *nekl-4* plus a 1609bp upstream promoter region was amplified from genomic DNA using primers with homology to pPD95.75 containing *gfp*. The stop codon for *nekl-4* was removed using the reverse primer. pPD95.75 was amplified using primers with homology to *nekl-4*. Fragments were joined using Gibson assembly [106].

genomic nekl-4 amplification (forward)	GATACGCTAACAACTTGGAAATGAAATagtagctggatgacgactgg
genomic nekl-4 amplification (reverse)	ggtcctcctgaaaatgttctatgttatgTCcCTTCGCTGCTGGATTTTC
pPD95.75 amplification (forward)	GAAAATCCAGCAGCGAAGgGAcataacatagaacattttcaggaggacc
pPD95.75 amplification (reverse)	ccagtcgtcatccagctactATTTCATTTCCAAGTTGTTAGCGTATC

https://doi.org/10.1371/journal.pgen.1009052.t001

CRISPR constructs

For creation of the *nekl-4*::*mneongreen* and *nekl-4*::*mscarlet-I* endogenous CRISPR tags, we followed the Mello Lab protocol [107] and used pdsDNA [108] that included a short flexible linker sequence between the 3' end of *nekl-4* and the start of *mneongreen* or *mscarlet-I*. The guide sequence was designed using CRISPOR [109,110] and silent mutation sites for PAM modification and diagnosis were located using WatCut silent mutation scanning [111]. Reagents used are as follows. dg357 was a gift from Dominique A. Glauser and was used in accordance with the *C. elegans* group license with AlleleBiotech. pSEM90 was a gift from Thomas Boulin.

mNeonGreen amplification from	
dg357 (forward) for donor	TGTCAGCGTGCATTGAATGTTTGATTGCAGAAAATCCA
	GCCGCTAAAGGAGGTGGCGGATCTGGAGGTGGAGGCTCTG GAGGAGGTGGATCTATGGTGTCGAAGGGAGAAG
mNeonGreen amplification from	
dg357 (reverse) for donor	
	TATACAAAAAAACAGTATATACAATTTAGCATATGCTACTTGTAGAGTTCATCCATTC
mScarlet-I amplification from	
pSEM90 (forward) for donor	
	TGTCAGCGTGCATTGAATGTTTGATTGCAGAAAATCCAGCCG CTAAAGGAGGTGGCGGATCTGGAGGTGGAGGCTCTGGAGGAGGTGGATCTATGGTCAGCAAGGGAGAGG
mScarlet-I amplification from	
pSEM90 (reverse) for donor	
	TATACAAAAAAACAGTATATACAATTTAGCATATGCTACTTGTAGAGCTCGTCCATTCC
crRNA (reverse strand)	AGCAUAUGUCACUUCGCUGC

https://doi.org/10.1371/journal.pgen.1009052.t002

Supporting information

S1 Fig. Candidate gene mutations that did not suppress the *ccpp-1* dye-filling defect. For experiments involving the *mei-1(or1178)* temperature-sensitive allele, eggs from plates kept at the permissive temperature (15˚C; [112]) were picked to fresh plates and shifted to 25˚C after hatching for 4 days before scoring.
(TIF)

S2 Fig. Alignment of *C. elegans* NEKL-4 and human NEK10 kinase domains.
(TIF)

S3 Fig. NEKL-4 is localized to specialized ciliated sensory neurons in the male tail. a-b. Localization of NEKL-4::mNeonGreen in adult males. Tail is flat against the coverslip in **a.** to visualize ray dendrites. Tail in **b.** is folded but the filamentous pattern in ray cell bodies is visible. **c-d.** Localization of NEKL-4::mNeonGreen in L4 molt males. Both images are different sections from the same z-stack. Arrows indicate ray cell bodies, arrowheads indicate ray dendrites (numbered). Scale = 10μm.
(TIF)

S4 Fig. Examples of all genotypes scored for GT335 antibody staining in Fig 5. Scale bar = 10μm.
(TIF)

S5 Fig. Examination of mutants with polyE antibody, which detects side-chains of three or more glutamates. a. Example images of polyE stained cilia in the nose. The polyE polyclonal antibody stained amphid ciliary middle segments (MS) and labial and cephalic cilia (LC), similar to GT335. Abnormal polyE staining was visible in some strains containing the *ccpp-1* deletion mutation. Loss of TTLL-11 abolished polyE staining, but in the absence of TTLL-4 or TTLL-5, polyE staining remained. Scale = 10μm. **b**. Quantification of polyE staining phenotypes by genotype; number of animals examined indicated at right.
(TIF)

S1 Movie. NEKL-4::mNeonGreen movement in the amphid distal dendrites. Time lapse of a single z slice with widefield microscope. Images acquired at 4.34 fps and shown at 20 fps.
(MP4)

S1 Table. List of independent *ccpp-1* suppressor isolates. Strains contain the allele mentioned and the *ccpp-1(ok1821)* deletion. At least 20 animals were tested for Dye filling for each strain. Although a single P_0 plate produced *my42* and *my43*, we considered them independent isolates because their phenotypes are different from one another.
(XLSX)

S2 Table. Mutations examined in this study. GKO; Gene Knockout Consortium. CGC; Caenorhabditis Genetics Center. NBRP; National Bio-Resource Project.
(XLSX)

S3 Table. Summary of suppression of *ccpp-1* phenotypes by mutations examined in this study. + indicates any degree of suppression of the *ccpp-1* phenotype,—indicates no suppression of the *ccpp-1* phenotype, n/a indicates not tested.
(XLSX)

S4 Table. Potential NEKL-4 substrates. Based on phosphoproteomics data for NEK10 from Chivukula *et al*, Fig 4F [26]. Original list contains genes with phosphopeptides depleted more than twofold upon NEK10 deletion in human bronchial epithelial cell (HBEC) culture. This list contains genes with known *C. elegans* homologs from the following relevant classes in the NEK10 list: axonemal dyneins and assembly factors, kinesins, intraflagellar transport, ciliary length control.
(XLSX)

S5 Table. Strains used in this work. All strains were generated in the Barr laboratory except CB1490 (Hodgkin laboratory), ROH11 and ROH12 (O'Hagan laboratory).
(XLSX)

S6 Table. Strains used in supplemental material. All strains were generated in the Barr laboratory except BS3383, which was obtained from the Caenorhabditis Genetics Center (CGC).
(XLSX)

S1 Reference. Supplemental References.
(DOCX)

Acknowledgments

We thank members of the Barr lab, the Rutgers University *C. elegans* community, and K. M. P.'s thesis committee Marc Gartenberg, Monica Driscoll, and Bonnie Firestein for advice and

helpful feedback; Antonina Roll-Mecak for insight on TTLL-5 structure; and Helen Ushakov and Gloria Androwski for technical assistance. We thank Dominique A. Glauser and Thomas Boulin for plasmids. We also thank WormBase (U41 HG002223) and WormAtlas (R24 OD010943) for online resources. Some strains were provided by the CGC, which is funded by NIH Office of Research Infrastructure Programs (P40 OD010440), or by the National Bio-Resource Project of the MEXT, Japan.

Author Contributions

Conceptualization: Kade M. Power, Maureen M. Barr, Robert O'Hagan.

Data curation: Kade M. Power, Maureen M. Barr.

Formal analysis: Kade M. Power, Jyothi S. Akella, Amanda Gu, Jonathon D. Walsh, Sebastian Bellotti, Margaret Morash, Winnie Zhang, Yasmin H. Ramadan, Nicole Ross, Andy Golden, Harold E. Smith, Maureen M. Barr, Robert O'Hagan.

Funding acquisition: Maureen M. Barr, Robert O'Hagan.

Investigation: Kade M. Power, Amanda Gu, Jonathon D. Walsh, Sebastian Bellotti, Margaret Morash, Winnie Zhang, Yasmin H. Ramadan, Nicole Ross, Andy Golden, Harold E. Smith, Maureen M. Barr, Robert O'Hagan.

Methodology: Kade M. Power, Maureen M. Barr, Robert O'Hagan.

Project administration: Maureen M. Barr, Robert O'Hagan.

Resources: Andy Golden, Harold E. Smith, Maureen M. Barr, Robert O'Hagan.

Supervision: Maureen M. Barr, Robert O'Hagan.

Validation: Kade M. Power, Robert O'Hagan.

Visualization: Kade M. Power, Jyothi S. Akella, Maureen M. Barr.

Writing – original draft: Kade M. Power, Jyothi S. Akella, Maureen M. Barr, Robert O'Hagan.

Writing – review & editing: Kade M. Power, Jyothi S. Akella, Maureen M. Barr, Robert O'Hagan.

References

1. Reiter JF, Leroux MR. Genes and molecular pathways underpinning ciliopathies. Nat Rev Mol Cell Biol. 2017; 18: 533–547. https://doi.org/10.1038/nrm.2017.60 PMID: 28698599
2. Verhey KJ, Gaertig J. The tubulin code. Cell Cycle. 2007; 6: 2152–2160. https://doi.org/10.4161/cc.6.17.4633 PMID: 17786050
3. Magiera MM, Bodakuntla S, Žiak J, Lacomme S, Marques Sousa P, Leboucher S, et al. Excessive tubulin polyglutamylation causes neurodegeneration and perturbs neuronal transport. EMBO J. 2018;37. https://doi.org/10.15252/embj.2018100440 PMID: 30420556
4. Bodakuntla S, Schnitzler A, Villablanca C, Gonzalez-Billault C, Bieche I, Janke C, et al. Tubulin polyglutamylation is a general traffic control mechanism in hippocampal neurons. J Cell Sci. 2020. https://doi.org/10.1242/jcs.241802 PMID: 31932508
5. Rogowski K, van Dijk J, Magiera MM, Bosc C, Deloulme J-C, Bosson A, et al. A family of protein-deglutamylating enzymes associated with neurodegeneration. Cell. 2010; 143: 564–578. https://doi.org/10.1016/j.cell.2010.10.014 PMID: 21074048
6. Kimura Y, Kurabe N, Ikegami K, Tsutsumi K, Konishi Y, Kaplan OI, et al. Identification of tubulin deglutamylase among Caenorhabditis elegans and mammalian cytosolic carboxypeptidases (CCPs). J Biol Chem. 2010; 285: 22936–22941. https://doi.org/10.1074/jbc.C110.128280 PMID: 20519502

7. Janke C, Rogowski K, Wloga D, Regnard C, Kajava AV, Strub J-M, et al. Tubulin polyglutamylase enzymes are members of the TTL domain protein family. Science. 2005; 308: 1758–1762. https://doi.org/10.1126/science.1113010 PMID: 15890843
8. Ikegami K, Mukai M, Tsuchida J-I, Heier RL, Macgregor GR, Setou M. TTLL7 is a mammalian beta-tubulin polyglutamylase required for growth of MAP2-positive neurites. J Biol Chem. 2006; 281: 30707–30716. https://doi.org/10.1074/jbc.M603984200 PMID: 16901895
9. van Dijk J, Rogowski K, Miro J, Lacroix B, Eddé B, Janke C. A targeted multienzyme mechanism for selective microtubule polyglutamylation. Mol Cell. 2007; 26: 437–448. https://doi.org/10.1016/j.molcel.2007.04.012 PMID: 17499049
10. Garnham CP, Roll-Mecak A. The chemical complexity of cellular microtubules: tubulin post-translational modification enzymes and their roles in tuning microtubule functions. Cytoskeleton. 2012; 69: 442–463. Available: https://doi.org/10.1002/cm.21027 PMID: 22422711
11. Mullen RJ. Site of pcd gene action and Purkinje cell mosaicism in cerebella of chimaeric mice. Nature. 1977; 270: 245–247. https://doi.org/10.1038/270245a0 PMID: 593342
12. Landis SC, Mullen RJ. The development and degeneration of Purkinje cells in pcd mutant mice. J Comp Neurol. 1978; 177: 125–143. https://doi.org/10.1002/cne.901770109 PMID: 200636
13. Fernandez-Gonzalez A. Purkinje cell degeneration (pcd) Phenotypes Caused by Mutations in the Axotomy-Induced Gene, Nna1. Science. 2002. pp. 1904–1906. https://doi.org/10.1126/science.1068912 PMID: 11884758
14. Lee JE, Silhavy JL, Zaki MS, Schroth J, Bielas SL, Marsh SE, et al. CEP41 is mutated in Joubert syndrome and is required for tubulin glutamylation at the cilium. Nat Genet. 2012; 44: 193–199. https://doi.org/10.1038/ng.1078 PMID: 22246503
15. Brady ST, Morfini GA. Regulation of motor proteins, axonal transport deficits and adult-onset neurodegenerative diseases. Neurobiol Dis. 2017; 105: 273–282. https://doi.org/10.1016/j.nbd.2017.04.010 PMID: 28411118
16. Alexander AG, Marfil V, Li C. Use of Caenorhabditis elegans as a model to study Alzheimer's disease and other neurodegenerative diseases. Front Genet. 2014; 5: 279. https://doi.org/10.3389/fgene.2014.00279 PMID: 25250042
17. Ward S, Thomson N, White JG, Brenner S. Electron microscopical reconstruction of the anterior sensory anatomy of the nematodecaenorhabditis elegans. The Journal of Comparative Neurology. 1975. pp. 313–337. https://doi.org/10.1002/cne.901600305 PMID: 1112927
18. Perkins LA, Hedgecock EM, Nichol Thomson J, Culotti JG. Mutant sensory cilia in the nematode Caenorhabditis elegans. Developmental Biology. 1986. pp. 456–487. https://doi.org/10.1016/0012-1606(86)90314-3 PMID: 2428682
19. Ware RW, Clark D, Crossland K, Russell RL. The nerve ring of the nematodeCaenorhabditis elegans: Sensory input and motor output. The Journal of Comparative Neurology. 1975. pp. 71–110. https://doi.org/10.1002/cne.901610107 PMID: 1133228
20. Evans JE, Snow JJ, Gunnarson AL, Ou G, Stahlberg H, McDonald KL, et al. Functional modulation of IFT kinesins extends the sensory repertoire of ciliated neurons in Caenorhabditis elegans. The Journal of Cell Biology. 2006. pp. 663–669. https://doi.org/10.1083/jcb.200509115 PMID: 16492809
21. O'Hagan R, Piasecki BP, Silva M, Phirke P, Nguyen KCQ, Hall DH, et al. The tubulin deglutamylase CCPP-1 regulates the function and stability of sensory cilia in C. elegans. Curr Biol. 2011; 21: 1685–1694. https://doi.org/10.1016/j.cub.2011.08.049 PMID: 21982591
22. O'Hagan R, Silva M, Nguyen KCQ, Zhang W, Bellotti S, Ramadan YH, et al. Glutamylation Regulates Transport, Specializes Function, and Sculpts the Structure of Cilia. Curr Biol. 2017; 27: 3430–3441.e6. https://doi.org/10.1016/j.cub.2017.09.066 PMID: 29129530
23. Sergouniotis PI, Chakarova C, Murphy C, Becker M, Lenassi E, Arno G, et al. Biallelic variants in TTLL5, encoding a tubulin glutamylase, cause retinal dystrophy. Am J Hum Genet. 2014; 94: 760–769. https://doi.org/10.1016/j.ajhg.2014.04.003 PMID: 24791901
24. Sun X, Park JH, Gumerson J, Wu Z, Swaroop A, Qian H, et al. Loss of RPGR glutamylation underlies the pathogenic mechanism of retinal dystrophy caused by TTLL5 mutations. Proc Natl Acad Sci U S A. 2016; 113: E2925–34. https://doi.org/10.1073/pnas.1523201113 PMID: 27162334
25. Porpora M, Sauchella S, Rinaldi L, Delle Donne R, Sepe M, Torres-Quesada O, et al. Counterregulation of cAMP-directed kinase activities controls ciliogenesis. Nat Commun. 2018; 9: 1224. https://doi.org/10.1038/s41467-018-03643-9 PMID: 29581457
26. Chivukula RR, Montoro DT, Leung HM, Yang J, Shamseldin HE, Taylor MS, et al. A human ciliopathy reveals essential functions for NEK10 in airway mucociliary clearance. Nature Medicine. 2020. https://doi.org/10.1038/s41591-019-0730-x PMID: 31959991

27. Bompard G, van Dijk J, Cau J, Lannay Y, Marcellin G, Lawera A, et al. CSAP Acts as a Regulator of TTLL-Mediated Microtubule Glutamylation. Cell Rep. 2018; 25: 2866–2877.e5. https://doi.org/10.1016/j.celrep.2018.10.095 PMID: 30517872

28. Chawla DG, Shah RV, Barth ZK, Lee JD, Badecker KE, Naik A, et al. Caenorhabditis elegans glutamylating enzymes function redundantly in male mating. Biol Open. 2016; 5: 1290–1298. https://doi.org/10.1242/bio.017442 PMID: 27635036

29. WormBase: Nematode Information Resource. [cited 27 Jan 2020]. Available: https://wormbase.org//

30. T-Coffee Server. [cited 27 Jan 2020]. Available: http://tcoffee.crg.cat/apps/tcoffee/do:expresso

31. Wang J, Barr MM. Ciliary Extracellular Vesicles: Txt Msg Organelles. Cell Mol Neurobiol. 2016; 36: 449–457. https://doi.org/10.1007/s10571-016-0345-4 PMID: 26983828

32. Valenstein ML, Roll-Mecak A. Graded Control of Microtubule Severing by Tubulin Glutamylation. Cell. 2016; 164: 911–921. https://doi.org/10.1016/j.cell.2016.01.019 PMID: 26875866

33. Sharma N, Bryant J, Wloga D, Donaldson R, Davis RC, Jerka-Dziadosz M, et al. Katanin regulates dynamics of microtubules and biogenesis of motile cilia. J Cell Biol. 2007; 178: 1065–1079. https://doi.org/10.1083/jcb.200704021 PMID: 17846175

34. Ghosh-Roy A, Goncharov A, Jin Y, Chisholm AD. Kinesin-13 and tubulin posttranslational modifications regulate microtubule growth in axon regeneration. Dev Cell. 2012; 23: 716–728. https://doi.org/10.1016/j.devcel.2012.08.010 PMID: 23000142

35. Hatzfeld M. The armadillo family of structural proteins. Int Rev Cytol. 1999; 186: 179–224. https://doi.org/10.1016/s0074-7696(08)61054-2 PMID: 9770300

36. EMBOSS: epestfind. [cited 27 Jan 2020]. Available: http://emboss.bioinformatics.nl/cgi-bin/emboss/epestfind

37. Rogers S, Wells R, Rechsteiner M. Amino acid sequences common to rapidly degraded proteins: the PEST hypothesis. Science. 1986. pp. 364–368. https://doi.org/10.1126/science.2876518 PMID: 2876518

38. Altschul SF, Gish W, Miller W, Myers EW, Lipman DJ. Basic local alignment search tool. J Mol Biol. 1990; 215: 403–410. https://doi.org/10.1016/S0022-2836(05)80360-2 PMID: 2231712

39. Paix A, Folkmann A, Seydoux G. Precision genome editing using CRISPR-Cas9 and linear repair templates in C. elegans. Methods. 2017. pp. 86–93. https://doi.org/10.1016/j.ymeth.2017.03.023 PMID: 28392263

40. Dickinson DJ, Goldstein B. CRISPR-Based Methods for Caenorhabditis elegans Genome Engineering. Genetics. 2016. pp. 885–901. https://doi.org/10.1534/genetics.115.182162 PMID: 26953268

41. Yi P, Xie C, Ou G. The kinases male germ cell-associated kinase and cell cycle-related kinase regulate kinesin-2 motility in Caenorhabditis elegans neuronal cilia. Traffic. 2018; 19: 522–535. https://doi.org/10.1111/tra.12572 PMID: 29655266

42. Haycraft CJ, Schafer JC, Zhang Q, Taulman PD, Yoder BK. Identification of CHE-13, a novel intraflagellar transport protein required for cilia formation. Exp Cell Res. 2003; 284: 251–263. https://doi.org/10.1016/s0014-4827(02)00089-7 PMID: 12651157

43. Wolff A, de Néchaud B, Chillet D, Mazarguil H, Desbruyères E, Audebert S, et al. Distribution of glutamylated alpha and beta-tubulin in mouse tissues using a specific monoclonal antibody, GT335. Eur J Cell Biol. 1992; 59: 425–432. Available: https://www.ncbi.nlm.nih.gov/pubmed/1493808 PMID: 1493808

44. Pathak N, Obara T, Mangos S, Liu Y, Drummond IA. The Zebrafish fleer Gene Encodes an Essential Regulator of Cilia Tubulin Polyglutamylation. Molecular Biology of the Cell. 2007. pp. 4353–4364. https://doi.org/10.1091/mbc.e07-06-0537 PMID: 17761526

45. Silva M, Morsci N, Nguyen KCQ, Rizvi A, Rongo C, Hall DH, et al. Cell-Specific α-Tubulin Isotype Regulates Ciliary Microtubule Ultrastructure, Intraflagellar Transport, and Extracellular Vesicle Biology. Curr Biol. 2017; 27: 968–980. https://doi.org/10.1016/j.cub.2017.02.039 PMID: 28318980

46. Scholey JM, Ou G, Snow J, Gunnarson A. Intraflagellar transport motors in Caenorhabditis elegans neurons. Biochemical Society Transactions. 2004. pp. 682–684. https://doi.org/10.1042/BST0320682 PMID: 15493987

47. Ou G, Blacque OE, Snow JJ, Leroux MR, Scholey JM. Functional coordination of intraflagellar transport motors. Nature. 2005. pp. 583–587. https://doi.org/10.1038/nature03818 PMID: 16049494

48. Prevo B, Mangeol P, Oswald F, Scholey JM, Peterman EJG. Functional differentiation of cooperating kinesin-2 motors orchestrates cargo import and transport in C. elegans cilia. Nat Cell Biol. 2015; 17: 1536–1545. https://doi.org/10.1038/ncb3263 PMID: 26523365

49. Hao L, Efimenko E, Swoboda P, Scholey JM. The retrograde IFT machinery of C. elegans cilia: two IFT dynein complexes? PLoS One. 2011; 6: e20995. https://doi.org/10.1371/journal.pone.0020995 PMID: 21695221

50. Imanishi M, Endres NF, Gennerich A, Vale RD. Autoinhibition regulates the motility of the C. elegans intraflagellar transport motor OSM-3. The Journal of Cell Biology. 2006. pp. 931–937. https://doi.org/10.1083/jcb.200605179 PMID: 17000874

51. Kubo T, Yanagisawa H-A, Yagi T, Hirono M, Kamiya R. Tubulin polyglutamylation regulates axonemal motility by modulating activities of inner-arm dyneins. Curr Biol. 2010; 20: 441–445. https://doi.org/10.1016/j.cub.2009.12.058 PMID: 20188560

52. Lin H, Zhang Z, Guo S, Chen F, Kessler JM, Wang YM, et al. A NIMA-Related Kinase Suppresses the Flagellar Instability Associated with the Loss of Multiple Axonemal Structures. PLoS Genet. 2015; 11: e1005508. https://doi.org/10.1371/journal.pgen.1005508 PMID: 26348919

53. Cohen S, Aizer A, Shav-Tal Y, Yanai A, Motro B. Nek7 kinase accelerates microtubule dynamic instability. Biochim Biophys Acta. 2013; 1833: 1104–1113. https://doi.org/10.1016/j.bbamcr.2012.12.021 PMID: 23313050

54. Wloga D, Camba A, Rogowski K, Manning G, Jerka-Dziadosz M, Gaertig J. Members of the NIMA-related Kinase Family Promote Disassembly of Cilia by Multiple Mechanisms. Molecular Biology of the Cell. 2006. pp. 2799–2810. https://doi.org/10.1091/mbc.e05-05-0450 PMID: 16611747

55. Chaya T, Omori Y, Kuwahara R, Furukawa T. ICK is essential for cell type-specific ciliogenesis and the regulation of ciliary transport. EMBO J. 2014; 33: 1227–1242. https://doi.org/10.1002/embj.201488175 PMID: 24797473

56. Luo M, Cao M, Kan Y, Li G, Snell W, Pan J. The phosphorylation state of an aurora-like kinase marks the length of growing flagella in Chlamydomonas. Curr Biol. 2011; 21: 586–591. https://doi.org/10.1016/j.cub.2011.02.046 PMID: 21458267

57. Pan J, Wang Q, Snell WJ. An aurora kinase is essential for flagellar disassembly in Chlamydomonas. Dev Cell. 2004; 6: 445–451. https://doi.org/10.1016/s1534-5807(04)00064-4 PMID: 15030766

58. Liang Y, Pang Y, Wu Q, Hu Z, Han X, Xu Y, et al. FLA8/KIF3B phosphorylation regulates kinesin-II interaction with IFT-B to control IFT entry and turnaround. Dev Cell. 2014; 30: 585–597. https://doi.org/10.1016/j.devcel.2014.07.019 PMID: 25175706

59. van de Kooij B, Creixell P, van Vlimmeren A, Joughin BA, Miller CJ, Haider N, et al. Comprehensive substrate specificity profiling of the human Nek kinome reveals unexpected signaling outputs. Elife. 2019; 8. https://doi.org/10.7554/eLife.44635 PMID: 31124786

60. Monteiro MI, Ahlawat S, Kowalski JR, Malkin E, Koushika SP, Juo P. The kinesin-3 family motor KLP-4 regulates anterograde trafficking of GLR-1 glutamate receptors in the ventral nerve cord of Caenorhabditis elegans. Mol Biol Cell. 2012; 23: 3647–3662. https://doi.org/10.1091/mbc.E12-04-0334 PMID: 22855524

61. Lacroix B, Bourdages KG, Dorn JF, Ihara S, Sherwood DR, Maddox PS, et al. In situ imaging in C. elegans reveals developmental regulation of microtubule dynamics. Dev Cell. 2014; 29: 203–216. https://doi.org/10.1016/j.devcel.2014.03.007 PMID: 24780738

62. Ou G, Koga M, Blacque OE, Murayama T, Ohshima Y, Schafer JC, et al. Sensory ciliogenesis in Caenorhabditis elegans: assignment of IFT components into distinct modules based on transport and phenotypic profiles. Mol Biol Cell. 2007; 18: 1554–1569. https://doi.org/10.1091/mbc.e06-09-0805 PMID: 17314406

63. Bell LR, Stone S, Yochem J, Shaw JE, Herman RK. The molecular identities of the Caenorhabditis elegans intraflagellar transport genes dyf-6, daf-10 and osm-1. Genetics. 2006; 173: 1275–1286. https://doi.org/10.1534/genetics.106.056721 PMID: 16648645

64. Qin H, Rosenbaum JL, Barr MM. An autosomal recessive polycystic kidney disease gene homolog is involved in intraflagellar transport in C. elegans ciliated sensory neurons. Curr Biol. 2001; 11: 457–461. https://doi.org/10.1016/s0960-9822(01)00122-1 PMID: 11301258

65. Bae Y-K, Qin H, Knobel KM, Hu J, Rosenbaum JL, Barr MM. General and cell-type specific mechanisms target TRPP2/PKD-2 to cilia. Development. 2006; 133: 3859–3870. https://doi.org/10.1242/dev.02555 PMID: 16943275

66. Chen N, Mah A, Blacque OE, Chu J, Phgora K, Bakhoum MW, et al. Identification of ciliary and ciliopathy genes in Caenorhabditis elegans through comparative genomics. Genome Biol. 2006; 7: R126. https://doi.org/10.1186/gb-2006-7-12-r126 PMID: 17187676

67. Burghoorn J, Dekkers MPJ, Rademakers S, de Jong T, Willemsen R, Jansen G. Mutation of the MAP kinase DYF-5 affects docking and undocking of kinesin-2 motors and reduces their speed in the cilia of Caenorhabditis elegans. Proc Natl Acad Sci U S A. 2007; 104: 7157–7162. https://doi.org/10.1073/pnas.0606974104 PMID: 17420466

68. Maurya AK, Rogers T, Sengupta P. A CCRK and a MAK Kinase Modulate Cilia Branching and Length via Regulation of Axonemal Microtubule Dynamics in Caenorhabditis elegans. Current Biology. 2019. pp. 1286–1300.e4. https://doi.org/10.1016/j.cub.2019.02.062 PMID: 30955935

69. Joseph BB, Wang Y, Edeen P, Lažetić V, Grant BD, Fay DS. Control of clathrin-mediated endocytosis by NIMA family kinases. PLoS Genet. 2020; 16: e1008633. https://doi.org/10.1371/journal.pgen.1008633 PMID: 32069276

70. Lažetić V, Joseph BB, Bernazzani SM, Fay DS. Actin organization and endocytic trafficking are controlled by a network linking NIMA-related kinases to the CDC-42-SID-3/ACK1 pathway. PLOS Genetics. 2018. p. e1007313. https://doi.org/10.1371/journal.pgen.1007313 PMID: 29608564

71. Lažetić V, Fay DS. Conserved Ankyrin Repeat Proteins and Their NIMA Kinase Partners Regulate Extracellular Matrix Remodeling and Intracellular Trafficking in Caenorhabditis elegans. Genetics. 2017; 205: 273–293. https://doi.org/10.1534/genetics.116.194464 PMID: 27799278

72. Kaplan OI, Doroquez DB, Cevik S, Bowie RV, Clarke L, Sanders AAWM, et al. Endocytosis Genes Facilitate Protein and Membrane Transport in C. elegans Sensory Cilia. Curr Biol. 2012; 22: 451–460. https://doi.org/10.1016/j.cub.2012.01.060 PMID: 22342749

73. Vaart A van der, van der Vaart A, Rademakers S, Jansen G. DLK-1/p38 MAP Kinase Signaling Controls Cilium Length by Regulating RAB-5 Mediated Endocytosis in Caenorhabditis elegans. PLOS Genetics. 2015. p. e1005733. https://doi.org/10.1371/journal.pgen.1005733 PMID: 26657059

74. Kubo T, Hirono M, Aikawa T, Kamiya R, Witman GB. Reduced tubulin polyglutamylation suppresses flagellar shortness in Chlamydomonas. Mol Biol Cell. 2015; 26: 2810–2822. https://doi.org/10.1091/mbc.E15-03-0182 PMID: 26085508

75. Hao L, Thein M, Brust-Mascher I, Civelekoglu-Scholey G, Lu Y, Acar S, et al. Intraflagellar transport delivers tubulin isotypes to sensory cilium middle and distal segments. Nat Cell Biol. 2011; 13: 790–798. https://doi.org/10.1038/ncb2268 PMID: 21642982

76. Das A, Dickinson D, Wood C, Goldstein B, Slep KC. The CHE-12 protein family uses a TOG domain array to regulate microtubules in the primary cilium. MOLECULAR BIOLOGY OF THE CELL. AMER SOC CELL BIOLOGY 8120 WOODMONT AVE, STE 750, BETHESDA, MD 20814–2755 USA; 2014.

77. Sanders A, Cevik S, Kida K, Bowie R, Blacque O. Investigation of a novel cilia-related gene K04F10.2/KIAA0556 in C. elegans. Cilia. 2012. https://doi.org/10.1186/2046-2530-1-s1-p43

78. Chang J, Baloh RH, Milbrandt J. The NIMA-family kinase Nek3 regulates microtubule acetylation in neurons. J Cell Sci. 2009; 122: 2274–2282. https://doi.org/10.1242/jcs.048975 PMID: 19509051

79. O'regan L, Blot J, Fry AM. Mitotic regulation by NIMA-related kinases. Cell Div. 2007; 2: 25. https://doi.org/10.1186/1747-1028-2-25 PMID: 17727698

80. Jackson PK. Nek8 couples renal ciliopathies to DNA damage and checkpoint control. Molecular cell. 2013. pp. 407–408. https://doi.org/10.1016/j.molcel.2013.08.013 PMID: 23973371

81. Bryan MS, Argos M, Andrulis IL, Hopper JL, Chang-Claude J, Malone KE, et al. Germline Variation and Breast Cancer Incidence: A Gene-Based Association Study and Whole-Genome Prediction of Early-Onset Breast Cancer. Cancer Epidemiol Biomarkers Prev. 2018; 27: 1057–1064. https://doi.org/10.1158/1055-9965.EPI-17-1185 PMID: 29898891

82. Keller BM, McCarthy AM, Chen J, Armstrong K, Conant EF, Domchek SM, et al. Associations between breast density and a panel of single nucleotide polymorphisms linked to breast cancer risk: a cohort study with digital mammography. BMC Cancer. 2015; 15: 143. https://doi.org/10.1186/s12885-015-1159-3 PMID: 25881232

83. García-Díez I, Hernández-Muñoz I, Hernández-Ruiz E, Nonell L, Puigdecanet E, Bódalo-Torruella M, et al. Transcriptome and cytogenetic profiling analysis of matched in situ/invasive cutaneous squamous cell carcinomas from immunocompetent patients. Genes Chromosomes Cancer. 2019; 58: 164–174. Available: https://onlinelibrary.wiley.com/doi/abs/10.1002/gcc.22712 https://doi.org/10.1002/gcc.22712 PMID: 30474248

84. Casey JP, Brennan K, Scheidel N, McGettigan P, Lavin PT, Carter S, et al. Recessive NEK9 mutation causes a lethal skeletal dysplasia with evidence of cell cycle and ciliary defects. Hum Mol Genet. 2016; 25: 1824–1835. https://doi.org/10.1093/hmg/ddw054 PMID: 26908619

85. Mahjoub MR, Montpetit B, Zhao L, Finst RJ, Goh B, Kim AC, et al. The FA2 gene of Chlamydomonas encodes a NIMA family kinase with roles in cell cycle progression and microtubule severing during deflagellation. J Cell Sci. 2002; 115: 1759–1768. Available: https://www.ncbi.nlm.nih.gov/pubmed/11950892 PMID: 11950892

86. Bradley BA. A NIMA-related kinase, Cnk2p, regulates both flagellar length and cell size in Chlamydomonas. Journal of Cell Science. 2005. pp. 3317–3326. https://doi.org/10.1242/jcs.02455 PMID: 16030138

87. Westermann S, Weber K. Identification of CfNek, a novel member of the NIMA family of cell cycle regulators, as a polypeptide copurifying with tubulin polyglutamylation activity in Crithidia. J Cell Sci. 2002; 115: 5003–5012. https://doi.org/10.1242/jcs.00170 PMID: 12432086

88. Brenner S. The genetics of Caenorhabditis elegans. Genetics. 1974; 77: 71–94. Available: https://www.ncbi.nlm.nih.gov/pubmed/4366476 PMID: 4366476

89. WormBook. [cited 27 Jan 2020]. Available: http://wormbook.org/
90. Doitsidou M, Jarriault S, Poole RJ. Next-Generation Sequencing-Based Approaches for Mutation Mapping and Identification in Caenorhabditis elegans. Genetics. 2016; 204: 451–474. https://doi.org/10.1534/genetics.115.186197 PMID: 27729495
91. Wang Y, Wang JT, Rasoloson D, Stitzel ML, O' Connell KF, Smith HE, et al. Identification of suppressors of mbk-2/DYRK by whole-genome sequencing. G3. 2014; 4: 231–241. https://doi.org/10.1534/g3.113.009126 PMID: 24347622
92. Homer N. Bfast: Blat-like fast accurate search tool. 2009. Available: https://vcru.wisc.edu/simonlab/bioinformatics/programs/bfast/bfast-book.pdf
93. Li H, Handsaker B, Wysoker A, Fennell T, Ruan J, Homer N, et al. The Sequence Alignment/Map format and SAMtools. Bioinformatics. 2009. pp. 2078–2079. https://doi.org/10.1093/bioinformatics/btp352 PMID: 19505943
94. Wang K, Li M, Hakonarson H. ANNOVAR: functional annotation of genetic variants from high-throughput sequencing data. Nucleic Acids Res. 2010; 38: e164. https://doi.org/10.1093/nar/gkq603 PMID: 20601685
95. Huang S, Holt J, -Y. Kao C, McMillan L, Wang W. A novel multi-alignment pipeline for high-throughput sequencing data. Database. 2014. pp. bau057–bau057. https://doi.org/10.1093/database/bau057 PMID: 24948510
96. UniProt. [cited 27 Jan 2020]. Available: https://www.uniprot.org/
97. interpro7-client. [cited 27 Jan 2020]. Available: https://www.ebi.ac.uk/interpro/
98. ScanProsite. [cited 27 Jan 2020]. Available: https://prosite.expasy.org/scanprosite/
99. Protein BLAST: search protein databases using a protein query. [cited 27 Jan 2020]. Available: https://blast.ncbi.nlm.nih.gov/Blast.cgi?PAGE=Proteins
100. WormWeb.org—Exon-Intron Graphic Maker—by nikhil bhatla. [cited 27 Jan 2020]. Available: http://wormweb.org/exonintron
101. DOG 2.0—Protein Domain Structure Visualization. [cited 27 Jan 2020]. Available: http://dog.biocuckoo.org/
102. Ren J, Wen L, Gao X, Jin C, Xue Y, Yao X. DOG 1.0: illustrator of protein domain structures. Cell Res. 2009; 19: 271–273. https://doi.org/10.1038/cr.2009.6 PMID: 19153597
103. BoxShade Server. [cited 27 Jan 2020]. Available: https://embnet.vital-it.ch/software/BOX_form.html
104. Kimura Y, Tsutsumi K, Konno A, Ikegami K, Hameed S, Kaneko T, et al. Environmental responsiveness of tubulin glutamylation in sensory cilia is regulated by the p38 MAPK pathway. Sci Rep. 2018; 8: 8392. https://doi.org/10.1038/s41598-018-26694-w PMID: 29849065
105. ImageJ. [cited 27 Jan 2020]. Available: https://imagej.net/Welcome
106. Gibson DG, Young L, Chuang R-Y, Venter JC, Hutchison CA 3rd, Smith HO. Enzymatic assembly of DNA molecules up to several hundred kilobases. Nat Methods. 2009; 6: 343–345. https://doi.org/10.1038/nmeth.1318 PMID: 19363495
107. Dokshin GA, Ghanta KS, Piscopo KM, Mello CC. Robust Genome Editing with Short Single-Stranded and Long, Partially Single-Stranded DNA Donors in Caenorhabditis elegans. Genetics. 2018; 210: 781–787. https://doi.org/10.1534/genetics.118.301532 PMID: 30213854
108. Paix A, Folkmann A, Goldman DH, Kulaga H, Grzelak MJ, Rasoloson D, et al. Precision genome editing using synthesis-dependent repair of Cas9-induced DNA breaks. Proc Natl Acad Sci U S A. 2017; 114: E10745–E10754. https://doi.org/10.1073/pnas.1711979114 PMID: 29183983
109. Haeussler M, Schönig K, Eckert H, Eschstruth A, Mianné J, Renaud J-B, et al. Evaluation of off-target and on-target scoring algorithms and integration into the guide RNA selection tool CRISPOR. Genome Biol. 2016; 17: 148. https://doi.org/10.1186/s13059-016-1012-2 PMID: 27380939
110. CRISPOR. [cited 27 Jan 2020]. Available: http://crispor.tefor.net/
111. WatCut: An on-line tool for restriction analysis, silent mutation scanning, SNP-RFLP analysis. [cited 27 Jan 2020]. Available: http://watcut.uwaterloo.ca/template.php?act=silent_new
112. Connolly AA, Osterberg V, Christensen S, Price M, Lu C, Chicas-Cruz K, et al. Caenorhabditis elegans oocyte meiotic spindle pole assembly requires microtubule severing and the calponin homology domain protein ASPM-1. Mol Biol Cell. 2014; 25: 1298–1311. https://doi.org/10.1091/mbc.E13-11-0687 PMID: 24554763